April 2020

# Accurate Tracking of Position and Dose During VMAT Based On VMAT-CT

Xiaodong Zhao
*Louisiana State University and Agricultural and Mechanical College*

# ACCURATE TRACKING OF POSITION AND DOSE DURING VMAT BASED ON VMAT-CT

A Dissertation

Submitted to the Graduate Faculty of the
Louisiana State University and
Agricultural and Mechanical College
in partial fulfillment of the
requirements for the degree of
Doctor of Philosophy

in

The Department of Physics and Astronomy

by
Xiaodong Zhao
B.S., Nanjing University, 2014
May 2020

For my parents.

## ACKNOWLEDGEMENTS

I wish to thank my advisor, Dr. Rui Zhang, for teaching me about becoming a dedicated and committed physicist and researcher and I will always be proud to call him mentor. I am grateful to my advisory committee including Dr. Kenneth Matthews, Dr. Jonas Fontenot, Dr. James Matthews, and David Perrin, for their time and feedback on my project. Special thanks to Dr Kenneth Matthews for always encourage me through difficult times. Special thanks to Dr Jonas Fontenot for helping me with IRB study approval. Special thanks to David Perrin for always there to teach me clinical procedures and help me communicate with the therapists. I would like to thank Connel Chu for teaching me so much about the clinical work and always willing to help and always have new innovative ideas with whatever question I present. I would also like to thank Rebecca Guidry, for her constant positive energy in the clinic and help me so much with data collection in Covington. Additionally, many thanks to Frank Apollo for always helping me with dosimetry questions. I would also like to thank my classmates, Phillip Wall, Krystal Kirby, and John Doiron for their help going through these past six years. I also would like to thank my group members Jihyung Yoon, SA Yoganathan, Yibo Xie, Jackie Chen for helping me with different sorts of coding questions. I would also like to thank the therapists in Baton Rouge and Covington that helped me with data collection and patients that gave consent for our IRB study. Thank you to my parents, for their unconditional love and support, for always believing in me and always encouraging me through hard times in my life. Without them, I would not be where I am today.

# TABLE OF CONTENTS

# LIST OF TABLES

## LIST OF FIGURES

## ABSTRACT

Purpose: Local tomography reconstruction is achievable with EPID images acquired during VMAT and was named as VMAT-CT. However, it did not gain popularity due to multiple limitations and technical challenges. The goal of this study was to extend VMAT-CT concept, generate complete 3D or 4D CT images and dose, track and adapt VMAT plan based on updated images and dose.

Methods: We considered collimator angle and removed blurred areas in EPID images for VMAT-CT reconstruction to reduce artifacts and improve image quality. VMAT-CT+ images were generated by fusing VMAT-CT and planning CT using rigid or deformable registration. For 4D SBRT VMAT, breathing signal was extracted from EPID images which were sorted into four phases, and dose was calculated in each phase and registered to the mean position planning CT to generate 4D composite dose. Doses based on VMAT-CT+ and CBCT were compared for phantoms and real patients. When prescription dose was not met for PTV, re-planning was demonstrated on the phantoms. Possible uncertainties were also evaluated.

Results: Tracking based on VMAT-CT+ was accurate and superior to that based on CBCT since VMAT-CT+ can detect changes after setup. VMAT-CT could accurately detect phantom deformation and/or change of breathing pattern, and re-planning based on VMAT-CT could restore target coverage in both 3D and 4D cases. For the real patients, dose based on VMAT-CT agreed well with that based on CBCT acquired on the same day. The impact of uncertainties on dose was minimal for both 3D and 4D cases.

Conclusion: 3D and 4D tracking and adaptation of VMAT based on VMAT-CT are feasible. Our study can be incorporated into patients' daily routine and has the great potential to increase the confidence of beam delivery, catch and remedy errors during VMAT.

# 1. INTRODUCTION

## 1.1. Volumetric modulated arc therapy

Volumetric modulated arc therapy (VMAT), also called RapidArc, is one of the cutting-edge radiotherapy technologies for cancer treatment (Otto, 2008), and can be used to treat head and neck cancer, whole brain cancer, esophagus cancer, lung cancer, pancreatic cancer, prostate cancer and a wide variety of other cancerous tumor sites (Teoh *et al.*, 2013; Teoh *et al.*, 2011; Popple *et al.*, 2014; Ong *et al.*, 2010; Palma *et al.*, 2010; Verbakel *et al.*, 2009; Sapkaroski *et al.*, 2015). The goal of VMAT treatment is to deliver a highly conformal dose to the tumor region and spare the healthy organ around it. Dose rate, gantry speed, multi-leaf collimator (MLC) positions will dynamically vary during VMAT. There are two main vendors that manufacture linear accelerators (Linacs) that can deliver VMAT: Elekta (Elekta Oncology Systems, Crawley, UK) and Varian (Varian Oncology Systems, Palo Alto, CA). The machines used in this study are all Elekta operating at 6 MV.

There has been an increasing use of VMAT because it is a dynamic, highly conformal technique with a short treatment time (usually within two minutes). The advantages of a fast treatment include better positioning since patient will be less likely to move during treatment and high patient throughput. For example, stereotactic body radiation therapy (SBRT) is one of the most significant advances for treating localized diseases like non-small cell lung cancer, and VMAT is considered the best way to deliver it because of its short treatment time (Sapkaroski *et al.*, 2015).

However, VMAT contains high dose gradients and usually a high degree of complexity, and there is an increased requirement of accurate beam delivery and dose verification, especially if the tumor site is around an important organ like the spinal cord, or when the patient received

hypo-fractional radiotherapy such as SBRT. For SBRT lung treatments, the tumor is usually on the scale of 1 to 2 cm with a prescription dose of 10 Gy a fraction and five fractions in total. Patients will breathe during treatment, and their respiratory pattern during planning CT acquisition can differ from the breathing pattern during beam delivery. Moreover, the treatment can last up to 2 weeks, during which time the patients could go through anatomical change including weight loss and tumor shrinkage. SBRT VMAT is a complex treatment and dosimetric errors occur in one fraction can have a significant impact, so it needs effective monitoring and tracking methods.

### 1.2. Current quality assurance (QA) and tracking techniques

Patient-specific pre-treatment QA is routinely performed prior to the delivery of the first VMAT fraction to verify the individualized intensity modulated fields (Liang *et al.*, 2016; Ling *et al.*, 2008). Commonly, the individual fields are delivered, and planar dose maps are measured with ion chambers, diode arrays, film, or an electronic portal imaging device (EPID). The comparison of planned and measured doses is quantified by gamma analysis (Low *et al.*, 1998b). This evaluation index examines both the dose differences between measured and planned points and the distance-to-agreement (DTA), which is the distance to the nearest measured point that matches the planned dose. It can be calculated with the equation below,

$$\Gamma = \sqrt{\left(\frac{r}{\Delta d}\right)^2 + \left(\frac{\delta}{\Delta D}\right)^2} \tag{1}$$

where r represents the DTA, and $\delta$ represents the magnitude of the percent difference between the measured dose value and the planned dose value. Delta d and delta D are the required threshold agreement between the measured and planned dose distribution. For example, the clinical QA

thresholds at Mary Bird Perkins Cancer Center are 3%/3mm for the percent dose difference and DTA criteria, respectively.

Image guidance (Velec *et al.*), which is commonly employed to ensure proper patient position prior to each fraction. Image guidance is performed by aligning the images of the patient taken just prior to treatment with images used in the planning process. Current methods of image guidance include portal imaging, cone beam computed tomography (CBCT) (Figure 1.1.), megavoltage computed tomography, and stereoscopic x-ray imaging (Verellen *et al.*, 2007).

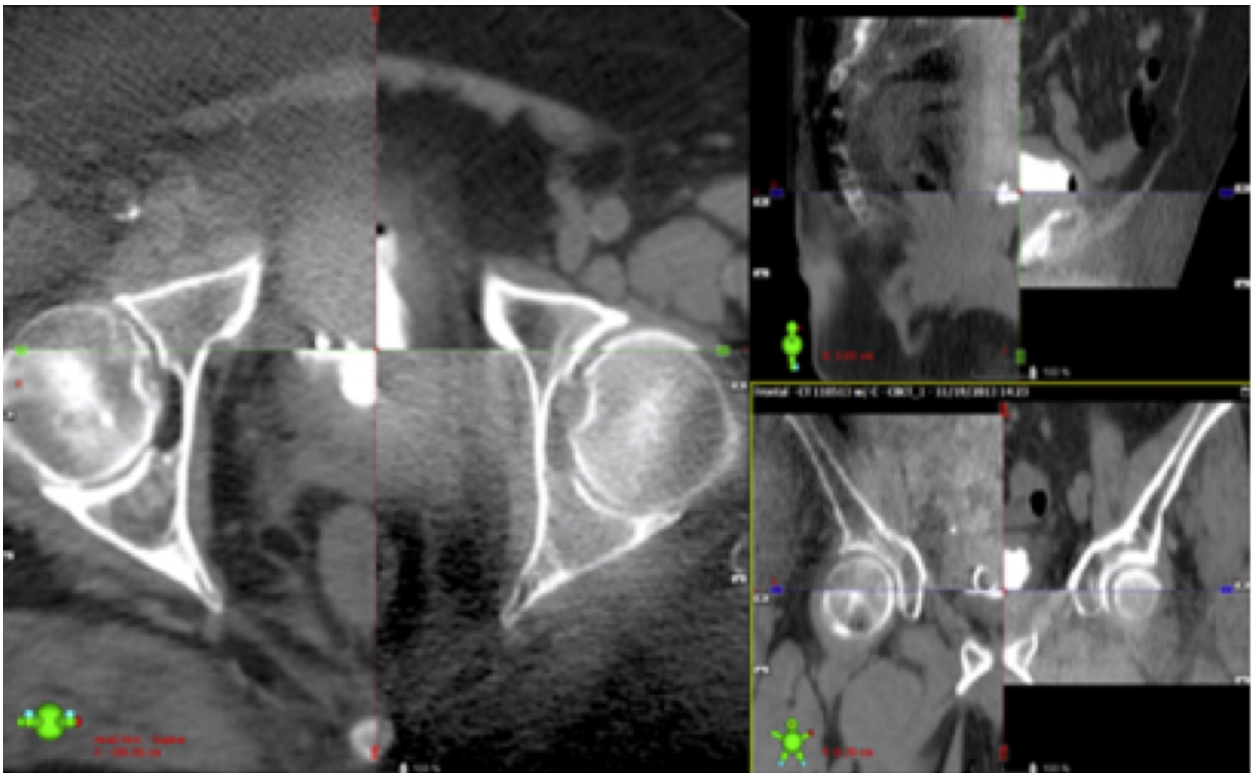

Figure 1.1. Cone beam CT fused with planning CT (Premo *et al.*, 2015)

Some of the IG techniques can only provide two-dimensional (2D) information like portal imaging and kV radiography. The other major concern for IG is the extra imaging dose, e.g. CBCT will introduce approximately 2~3 cGy in each fraction to healthy organs (Murphy *et al.*, 2007),

and four-dimensional (4D) CT or CBCT for patient's treatments that involve motion issue will introduce even higher dose to the patients (Cooper *et al.*, 2019b; Murphy *et al.*, 2007). The additional dose can elevate risks of side effects like secondary cancer for the patients (Murphy *et al.*, 2007; Goodman and Amurao, 2012; Lin, 2010; Ron, 2003; Chodick *et al.*, 2007; Ronckers *et al.*, 2010; Brenner *et al.*, 2003; Brenner *et al.*, 2001; Brenner and Elliston, 2004; Brenner and Hall, 2007), and it was estimated that approximately 2% of the cancers diagnosed annually in the US could be related to CT scans (Brenner and Hall, 2007), so attention to imaging exposure is vitally important.

Pre-treatment QA and IG can detect certain errors, but they are not sufficient to achieve "what you see is what you treat", i.e., they cannot detect intrafractional movement of the patient, changes in patient's anatomy or the errors during RT. Sometimes, a pre-treatment CBCT is compared with post-treatment CBCT to check if the patient moved during treatment, which would introduce extra imaging dose and still does not offer in-treatment geometry monitoring. In-treatment imaging modality is available in some cancer centers, but is not common in other cancer centers and also introduces extra imaging dose. Moreover, pre-treatment QA and IG cannot provide information on actual patient dose either. *In vivo* dosimetry has been used to supplement the weaknesses of pre-treatment QA and image guidance. Basically, dosimeters are generally placed on the surface of the patient to measure dose information during treatment. Thermoluminescent detectors (TLDs), optically stimulated luminescent dosimeter (OSLD), metal–oxide–semiconductor field-effect transistors, and silicon diodes are four varieties of dosimeters frequently used for in vivo dosimetry (Essers and Mijnheer, 1999; Bras and Pinho, 2015). However, measurement preparations and processing are laborious and time consuming for each dosimeter. More importantly, these methods generally provide dose information for only a

small number of points; a complete picture of the 3D dose distribution delivered to the patient is unobtainable.

## 1.3. Adaptive radiotherapy (ART)

The current shortcomings with QA and IGRT call for people's attention to verify the dose, and the need for ART. ART requires that a new treatment plan be made for the patient, which can occur at three different timescales: offline between fractions; online immediately prior to a fraction; in real time during a fraction (Kyoso, 2015). The process can be demonstrated in the Figure 1.2.: after patients' initial diagnostic CT image set was acquired and initial plan was approved, patients may start treatment. For online ART, patient would get an updated image set during each fraction of treatment. The initial image set would be registered to the new image set and adaptive re-planning would be carried out on the new image set and patients would be treated with an updated plan every fraction. For offline ART, adaptive re-planning usually happens after several fractions of treatment. The initial image set would be registered to the updated image set, and adaptive re-planning would be carried out on the new image set and patients would be treated with an updated plan after certain fractions of treatment.

ART aims to modify each patient's treatment plan based on patient-specific variation by evaluating and characterizing the systematic and random variations through image feedback and including them in adaptive planning. Accurate tracking of treatment and dose will significantly help clinicians determine when an art is needed. Dose reconstruction was usually done with CBCT or initial planning CT and log files (Lee *et al.*, 2008; Qian *et al.*, 2010). However, these are all done under the assumption that patient won't move during treatment because CBCT or initial planning CT is not taken during the treatment. Especially for lung cancer patients, the targeted

area may change drastically during the treatment. Additionally, CBCT would introduce extra imaging dose in each fraction.

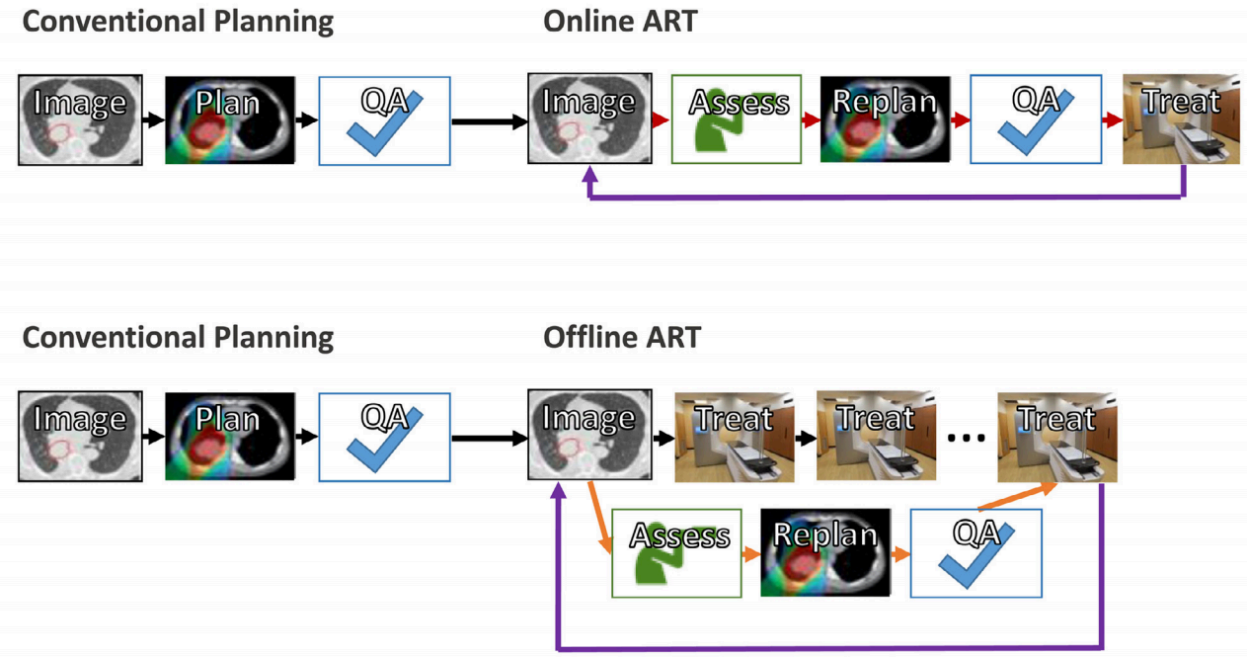


Figure 1.2. Workflow of ART(Green *et al.*, 2019)

## 1.4. Volumetric modulated arc therapy-computed tomography (VMAT-CT)

A CT scan combines a series of X-ray images taken from different angles and processes them to create cross-sectional views of the bones, blood vessels and soft tissues inside the body. CT reconstruction algorithms can be divided into 2 classes: (1) analytical methods, which includes Parallel beam reconstruction, i.e., Inverse-Radon Transform or Filtered Back Projection (DelPozo-Banos *et al.*, 2015), Fan beam reconstruction (DelPozo-Banos *et al.*, 2015), and FDK (Feldkamp, Davis, and Kress) algorithms for cone beam (Jin *et al.*, 2015); (2) Iterative reconstruction, which includes Statistical methods MLEM (Maximum Likelihood Estimation Method) (Bressane *et al.*, 2015), iterative methods with physical degradation correction such as motion, scatter and attenuation (Storisteanu *et al.*, 2015), and pure Bayesian methods like MCMC (Markov Chain Monte-Carlo) (Haghighat *et al.*, 2015).

Three-dimensional (3D) megavoltage (MV) CT reconstruction using portal images acquired during VMAT, so called "VMAT-CT", was first proposed by Poludniowski *et al.* in 2010 (Poludniowski *et al.*, 2010). To shape the beam from each gantry angle the same as the tumor shape projected to the detector panel at that angle, MLCs (multi-leaf collimator) are used to form field shapes designed specifically for each patient, which would introduce the problem of losing a lot of information during CT reconstruction. The data form an incomplete Radon transform of the subject and exact 'inversion' to reconstruct the patient is impossible (Poludniowski *et al.*, 2010). Poor image quality is an inherent characteristic of VMAT-CT compared to kV CT because of more scattering at MV energy. The loss of information from MLC blocking adds even more difficulty for reconstructing VMAT-CT images.

Poludniowski *et al.* (2010) showed even though the complete image reconstruction is not possible with the missing information due to MLC blockage, local VMAT-CT reconstruction is achievable with the modified global cone-beam filtered backprojection (FBP) algorithm, and this local reconstruction would help with position verification during treatment. The geometry of cone beam projected on EPID panel is shown in Figure 1.3. (Poludniowski *et al.*, 2010).

The FDK algorithm for cone beam reconstruction was proposed by Feldkamp, Davis, and Kress in 1984. It described an approximate reconstruction method for circular cone-beam tomography. It used small angle approximation so the reconstruction result would somewhat deviate from the measured object. Note that the FDK reconstruction algorithm is only an approximate formula for cone beam reconstruction. It can be shown that a single circular trajectory does not provide sufficient sampling for an exact cone beam reconstruction. Therefore, the algorithm performs reasonably well for small cone angles. When the cone angle becomes large, shading and streaking artifacts can occur (Tyldesley *et al.*, 2001; Kuse *et al.*, 2011). However, for

small cone angles, these deviations are usually considered small and acceptable. For the simplicity and fine math of FDK algorithm, it is the most commonly used reconstruction algorithm for cone beam CT (Jin *et al.*, 2015). The math of FDK algorithm can be expressed as:

$$f_R(r,\phi,z)=\frac{1}{2}\int_0^{2\pi} d\beta \left(\frac{\mathrm{SAD}}{\mathrm{SAD}-s}\right)^2 \int_{-u_{\max}}^{u_{\max}} du D_\beta(u,v) e_R(u'-u)\left(\frac{\mathrm{SAD}}{\sqrt{\mathrm{SAD}^2+u^2+v^2}}\right) \tag{2}$$

where,

$$u=U\left(\frac{\mathrm{SAD}}{\mathrm{SDD}}\right), \qquad v=V\left(\frac{\mathrm{SAD}}{\mathrm{SDD}}\right) \qquad u'=t\frac{\mathrm{SAD}}{\mathrm{SAD}-s} \qquad t=r\cos(\phi-\beta), \qquad s=r\sin(\phi-\beta)$$

where Dβ (u, v) is the cone-beam ray projection at the point on the detector defined by (u, v) for the source rotation, β (Poludniowski *et al.*, 2010). The other parameters are shown in the figure below.

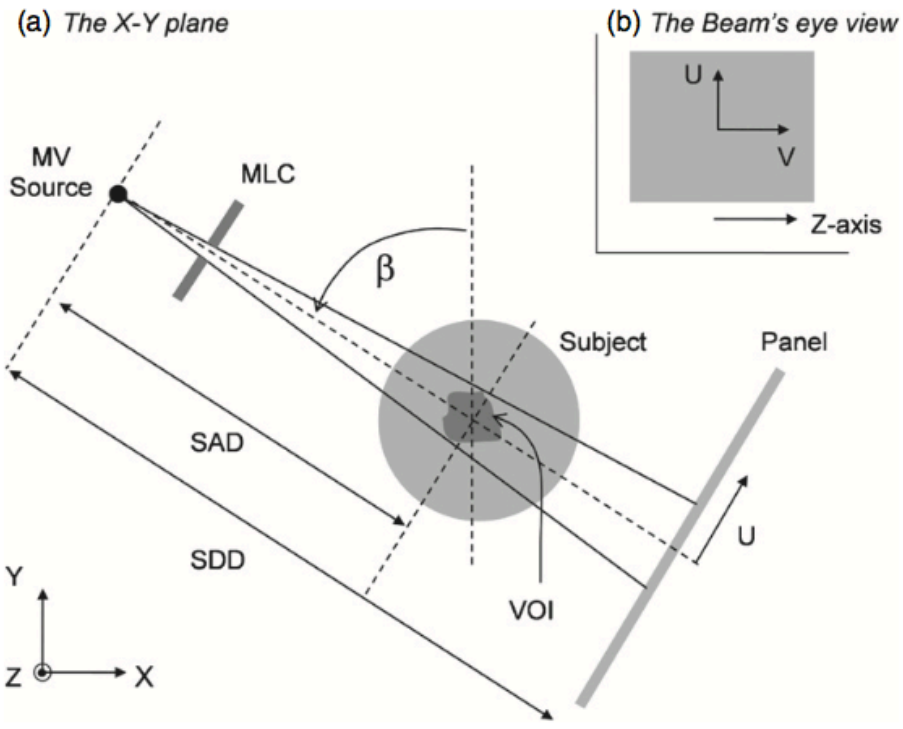


Figure 1.3. Geometry of MV cone beam projected on an EPID panel. The dark irregular shaded area is the tumor site to be reconstructed (Poludniowski *et al.*, 2010).

Poludniowski *et al.* (2010) modified the FDK algorithm used a local filter and a masking function. By extrapolating the image to outside the MLC region, they were able to get a back-projection with little to no streaking artifacts. By applying a masking function, regions outside the MLC opening would be excluded from the reconstruction. They also set up a threshold to exclude voxels that receive radiations less than certain threshold gantry angle (Poludniowski *et al.*, 2010). The final generalized version of the VMAT-CT reconstruction formula they proposed is

$$\Lambda^m f_R(r,\phi,z) \approx \frac{1}{2}\frac{\Theta\left(\int_0^{2\pi} M_\beta(u',v)\,\mathrm{d}\beta - \beta'\right)}{\frac{1}{2\pi}\int_0^{2\pi} M_\beta(u',v)\,\mathrm{d}\beta} \times \int_0^{2\pi}\left[M_\beta(u',v)\int_{-u_{\max}}^{u_{\max}} \mathrm{d}u\; D_\beta^{\mathrm{extrap}}(u,v)e_R^{(m)}(u'-u)\right]\mathrm{d}\beta, \tag{3}$$

where the local filter is

$$e_R^{(m)}(u) \approx \frac{1}{2\pi}\Lambda^{m+1}\varepsilon_R(u). \quad \Lambda\varepsilon(\underline{u}) = F^{-1}\{2\pi|\rho|F\{\varepsilon(\underline{u})\}\} \tag{4}$$

and

$$\begin{aligned}\varepsilon_R(u) &= \frac{1}{R\sqrt{\pi}}\frac{\Gamma\left(\frac{5}{2}+\alpha\right)}{\Gamma(2+\alpha)}\left(1-\left(\frac{u}{R}\right)^2\right)^{\alpha+1}, \qquad \text{if} \quad |u| \leqslant R \\ &= 0, \quad \text{otherwise,}\end{aligned} \tag{5}$$

where F is Fourier transform, $R$ defines a range, which is the support of PSF and $\alpha = 11.4174$ (Faridani *et al.*, 2001).

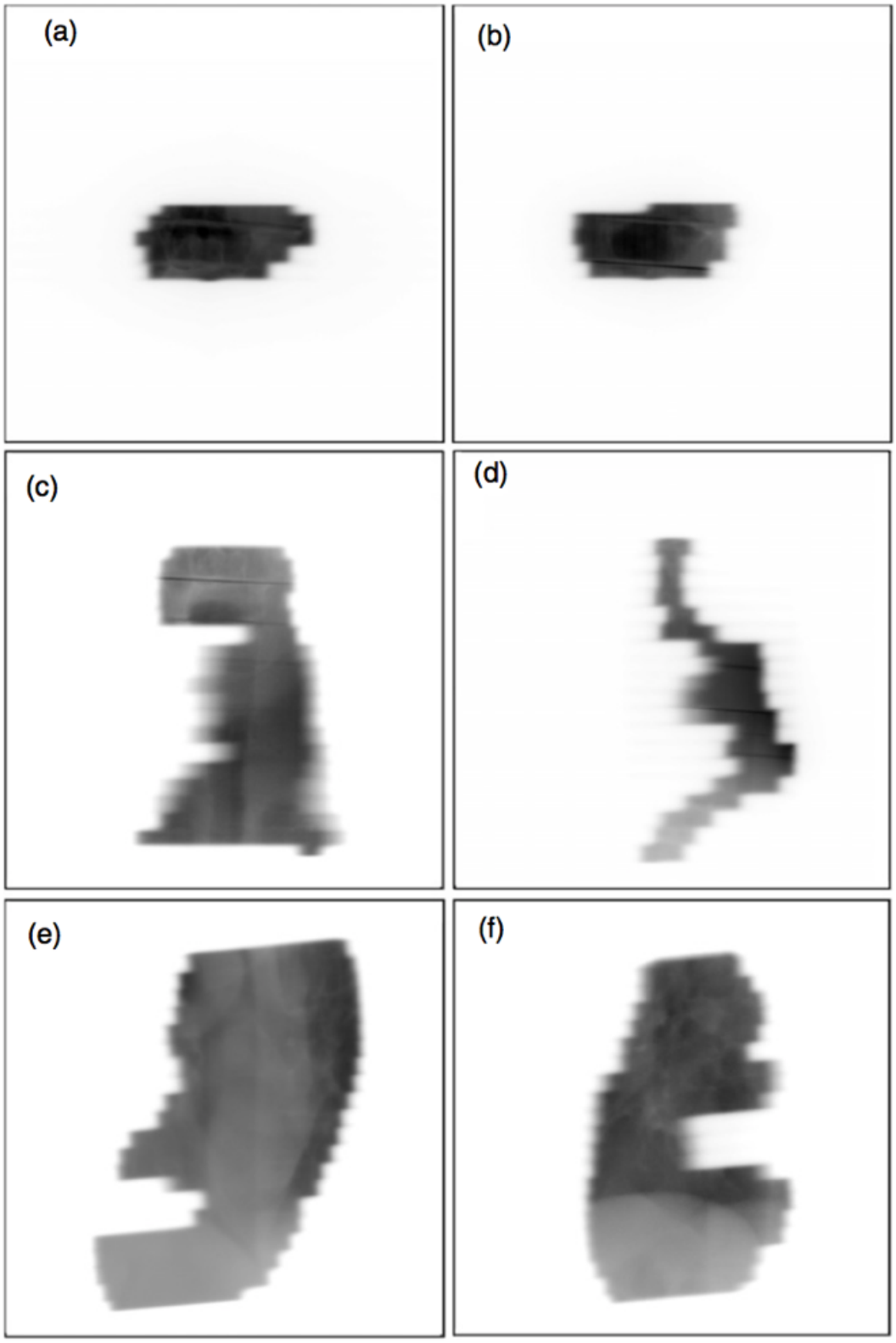


Figure 1.4. EPID images from different VMAT plans (Poludniowski *et al.*, 2010)

And some of the reconstruction results on a phantom are shown in Figure 1.5.:

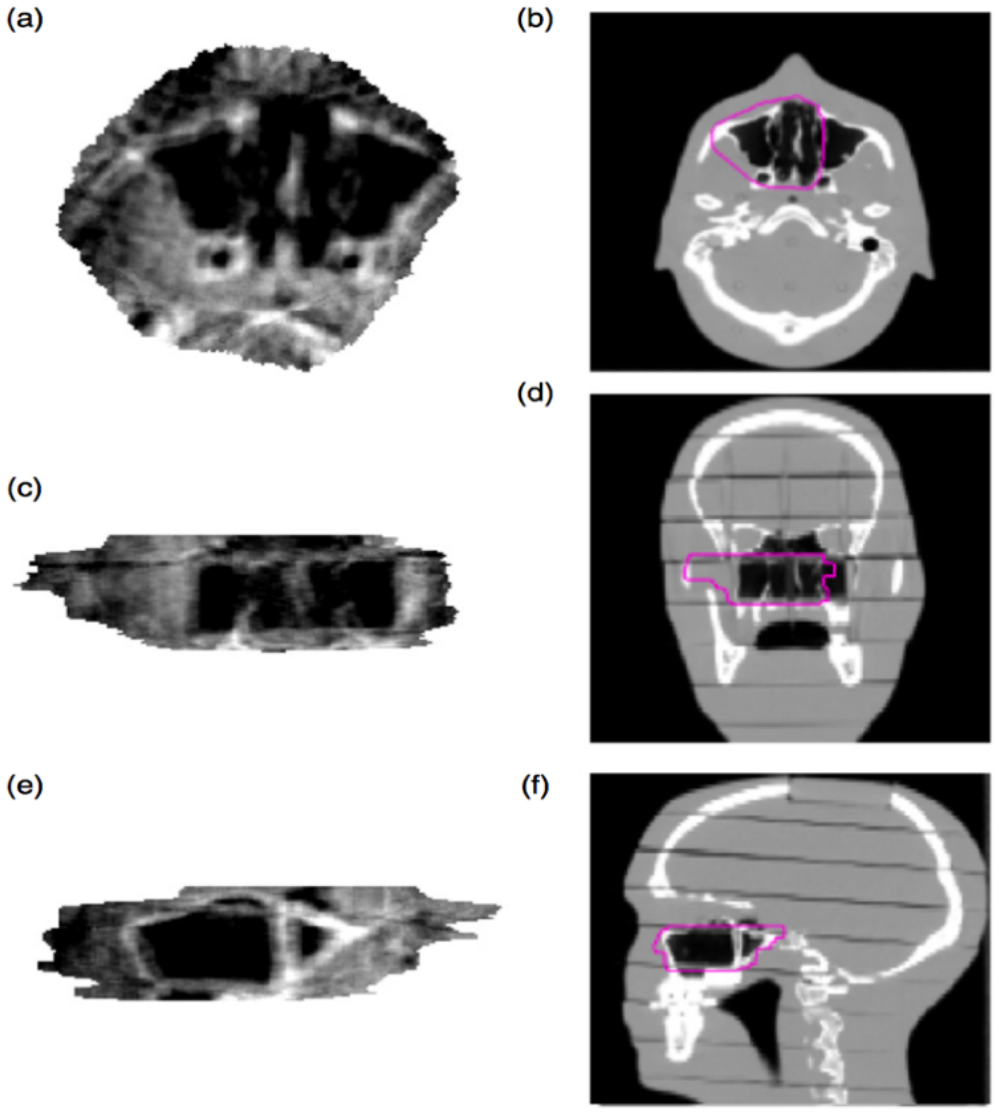


Figure 1.5. Reconstruction result for an antrum treatment (Poludniowski *et al.*, 2010)

Kida *et al.* (2011) developed a 4D version of VMAT-CT following the concept proposed by Poludniowski *et al* (2010). They compared two tracking methods that were based on 4D VMAT-CT and in-treatment kV CBCT for two patients, and a constraint on MLC motion of 0.1 cm/degree was applied to ensure target was always exposed during treatment, which is not

clinically realistic. The 4D VMAT-CT reconstruction results and the comparison to the in-treatment 4D CBCT for a patient are shown in Figure 1.6.:

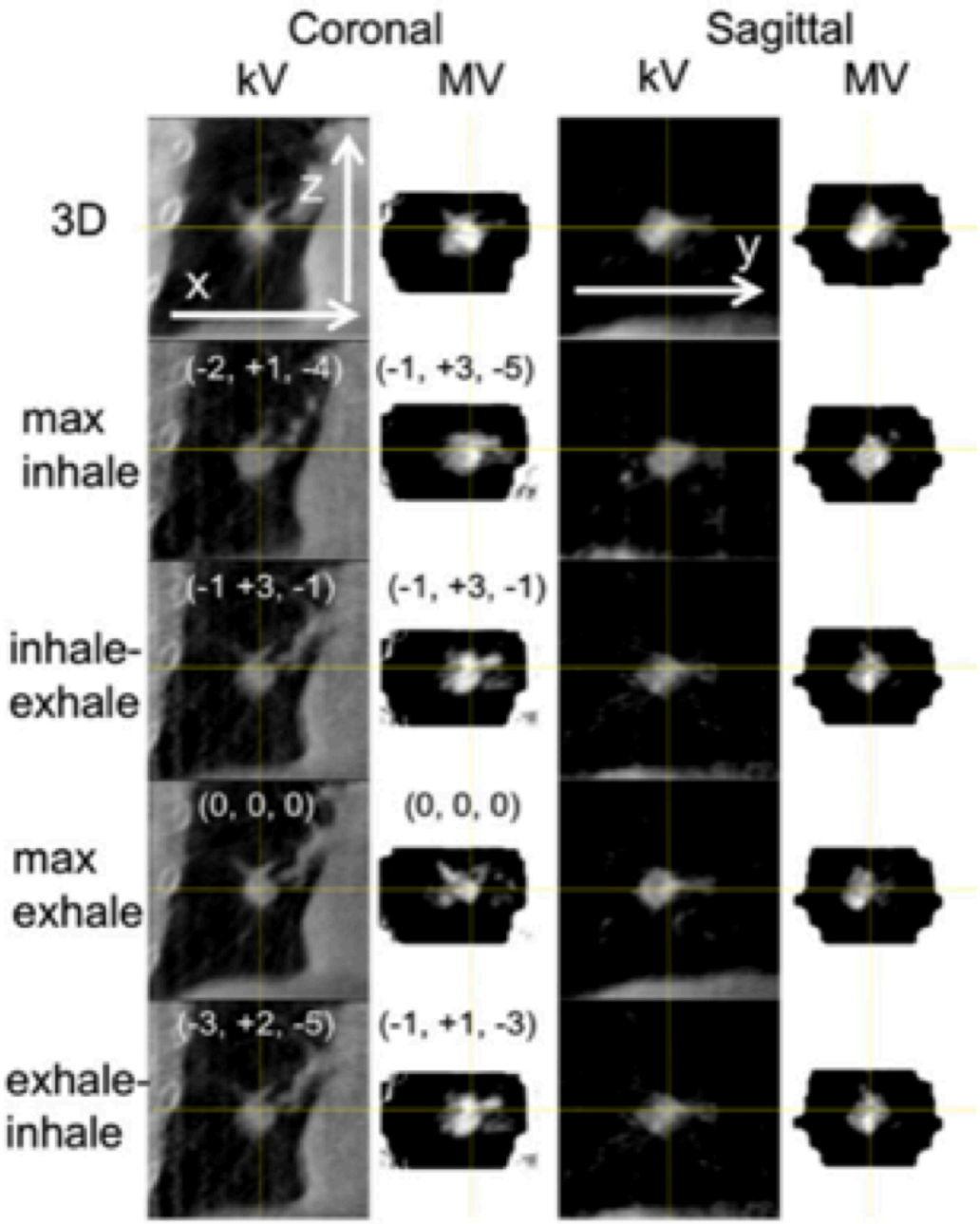


Figure 1.6. 4D VMAT-CT reconstruction result for 4D lung treatment compared to in-treatment 4D CBCT (Kida *et al.*, 2011).

## 1.5. Motivation, hypothesis and aims

Pre-treatment quality assurance (QA) and image guidance radiotherapy (IGRT) can detect certain errors, but they are not sufficient to detect intra-fractional movement of the patient or change of patient's anatomy or the errors after patient setup and during treatment. Especially for lung patients, they subject to breathing pattern change and it is very important to track the tumor position during SBRT lung treatments to make sure the patient's tumor is within the margin decided in the original treatment plan. They also cannot provide information on actual patient dose, and IGRT can induce extra imaging dose, e.g. CBCT taken before each treatment session can introduce 2 to 3 cGy extra dose to the patient each time. However, reconstruction of 3D or 4D VMAT-CT would introduce zero extra imaging dose since the EPID images come directly from the treatment beam. VMAT-CT provides real-time patient information during the treatment and dose delivered to the patient, and has the potential for accurate treatment tracking and ART. However, there are still some shortcomings of VMAT-CT like limited field of view (FOV), low image quality, and no electron density information. In addition, ART based on VMAT-CT has not been demonstrated.

The hypothesis of the study is for both 3D & 4D VMAT plans, position tracking and dose tracking by using the combination of VMAT-CT and planning CT is feasible and shows superior result than using CBCT. To test this hypothesis, comparison of geometry tracking and dose calculation based on VMAT-CT and CBCT were demonstrated on rigid phantom, in-house deformable phantom and real patients. We will test our hypothesis by performing the following aims: Aim 1. Feasibility of 3D tracking & adaptation based on VMAT-CT; Aim 2: Feasibility of 4D tracking & adaptation based on 4D VMAT-CT.

# 2. FEASIBILITY OF 3D TRACKING AND ADAPTATION OF VMAT BASED ON VMAT-CT

## 2.1. Introduction

Volumetric modulated arc therapy (VMAT) is an advanced technique that can deliver highly conformal radiation dose and reduce overall treatment time. However, due to high degree of complexity and dose gradients, the requirement of delivery accuracy has increased for VMAT. Pre-treatment quality assurance (QA) and image guidance can detect certain errors (Liang *et al.*, 2016; Ling *et al.*, 2008; Verellen *et al.*, 2007; Murphy *et al.*, 2007), but they are not sufficient to detect intra-fractional movement of the patient, change of patient's anatomy or the errors during VMAT, cannot provide information on actual patient dose, and image guidance can induce extra imaging dose to the patient (Murphy *et al.*, 2007). A few methods have been used to supplement QA and image guidance, including *in vivo* dosimetry (Mijnheer *et al.*, 2013) and machine log file monitoring (Tyagi *et al.*, 2012; Defoor *et al.*, 2015), but they also have limitations: conventional *in vivo* dosimetry is intrusive, time consuming and generally only provides point dose information; electronic portal imaging device (EPID) based *in vivo* dosimetry relies on back-projection dose reconstruction method which ignores the intra-fractional patient movement (Mans *et al.*, 2010); machine log file monitoring is also based on the assumption that patient does not move during the treatment (Tyagi *et al.*, 2012; Defoor *et al.*, 2015).

Adaptive radiotherapy (ART) holds the potential to compensate for the errors in treatment delivery by changing the treatment plan based on patient-specific variation during a treatment session (Li, 2011). Accurate tracking of treatment and dose will significantly help clinicians determine when an ART is needed. Initial planning computed tomography (Lu *et al.*) or cone beam CT (CBCT) were used for re-planning in most published ART studies (Qian *et al.*, 2010; Lee *et al.*, 2008). However, CBCT or planning CT and will introduce extra imaging dose and is not taken

during the treatment. ART based on these images cannot catch intra-fractional errors, and the actual dose delivered to the patient remains unknown.

Reconstruction of VMAT-CT was initially proposed in 2010 (Poludniowski *et al.*, 2010). It provides real-time patient information and would not increase imaging dose since the images come directly from treatment beams, but it has multiple shortcomings like limited field of view (FOV), low image quality, and no accurate density information. Poludniowski *et al.*'s study (2010) was based on Elekta MLCi2 MLCs which move relatively slower than the new Elekta Agility MLCs used in most current clinics. The faster MLC movement will further blur portal images and cause artifacts in VMAT-CT. In addition, 180$^{o}$ collimator angle was used in their study (2010), while any other angle could be used in patients' plans and cause artifacts in VMAT-CT. Our preliminary study also shows many VMAT plans cannot be reconstructed using a modified filtered backprojection (FBP) or local tomography algorithm proposed in 2010 study (Poludniowski *et al.*, 2010) due to highly modulated beams. Because of these disadvantages, VMAT-CT is not a well-established research area and there were very few follow-up studies (Kida *et al.*, 2011).

The goal of this study was to evaluate the feasibility of tracking three-dimensional (3D) VMAT treatment and dose considering intra-fractional movement using phantoms and adapting VMAT plan based on updated images and dose. This goal will be approached by combing VMAT-CT concept with improved image reconstruction methods and patient-specific prior information. Trackings based on VMAT-CT, planning CT and CBCT were compared. Criteria for VMAT-CT reconstruction and possible uncertainties associated with VMAT-CT were also evaluated.

## 2.2. Methods and Materials

### 2.2.1. Phantoms, Treatment Planning, and Data Collection

A Rando phantom was used for head and neck VMAT plan, and an Atom phantom was used for other sites including abdomen and prostate. The reason we did not include breast sites is because the beams were too big for the EPID panel. An in-house deformable lung phantom was created for this study as shown in Figure 2.1.: sponge inside a latex enclosure represented lungs, a small balloon filled with gel represented the deformable tumor, and the rest of the phantom was filled with rice powder to represent tissue. The deformable tumor was tied with strings on both sides: one side of it was fixed and the other side could be pulled to deform the tumor.

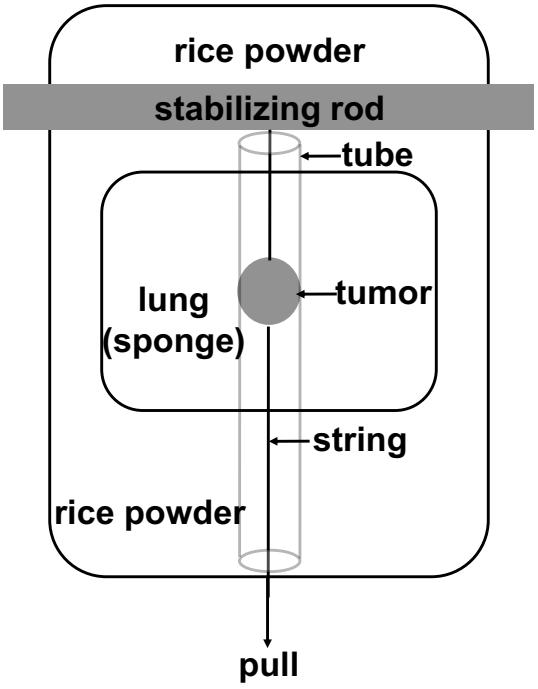


Figure 2.1. Descriptive figure of the in-house deformable lung phantom.

The VMAT plans were created in Pinnacle v9.10 treatment planning system (TPS) (Philips Medical Systems, Fitchburg, WI, USA), and were delivered using Elekta Versa Linac (Elekta Oncology Systems, Crawley, UK) operating at 6 MV. EPID images were acquired with iView in

movie mode and the frame averaging was set to be 1 to ensure maximum image counts. Timestamp associated with EPID images were also acquired within iView system. Meanwhile, gantry angles, monitor units (Low *et al.*) delivered, jaw position, and multi-leaf collimator (MLC) positions were recorded through Mobius log software (Mobius Medical Systems, Houston, TX).

Clinical head and neck, abdomen, and prostate VMAT plans were delivered to the Rando or Atom phantom with 600 MU/min dose rate, and a customized SBRT plan was delivered to the deformable lung phantom with 600 MU/min dose rate. For the head plan, the prescription dose was 40 Gy in 15 fractions, and 141 and 142 images were acquired from the two arcs with collimator angle 45$^{o}$ and 330$^{o}$, respectively. For the abdomen plan, the prescription dose was 48.6 Gy in 27 fractions, and 131 and 130 images were acquired from the two arcs with collimator angle 45$^{o}$ and 135$^{o}$, respectively. For the prostate plan, the prescription dose was 78 Gy in 39 fractions, and 140 and 135 images were acquired from the two arcs with collimator angle 45$^{o}$ and 315$^{o}$, respectively. For the SBRT lung plan, the prescription dose was 50 Gy in 5 fractions but only ¼ of a fraction's dose was delivered to reduce delivery time, and 57 and 56 images were acquired from the two arcs with collimator angle 45$^{o}$ and 165°, respectively.

The projection images consisted of 1024 ×1024 pixels with a resolution of 0.4 mm × 0.4 mm on EPID panel, which was projected to 0.25 mm × 0.25 mm at isocenter. Source to isocenter distance was 100 cm and source to EPID panel distance was 160 cm. MLC shapes derived from Linac log were matched with projection images to get the time difference between EPID images and Linac log. Gantry angle stored in the Linac log was then assigned to each projection image according to the time difference. All EPID images were normalized to the same scale so the maximum value in each image was 1, and were also corrected for any possible EPID displacement and gantry sagging.

2.2.2. VMAT-CT Reconstruction

Masking function and local tomography filter were adopted according to Poludniowski *et al.* (2010). Various collimator angles in clinical plans, i.e. the collimator angle in the plan we delivered could be 45°, 135°, 315°, and 330°, complicate the image extrapolation process: MLC leaves will move in a slanted direction in the X-Y plane when the collimator angle is not 180°, which may split the beam aperture into more than one connected region in the horizontal direction (u-direction) on EPID images (Figure 2.2.), reduce useful information in each region and cause streaking artifacts in VMAT-CT.

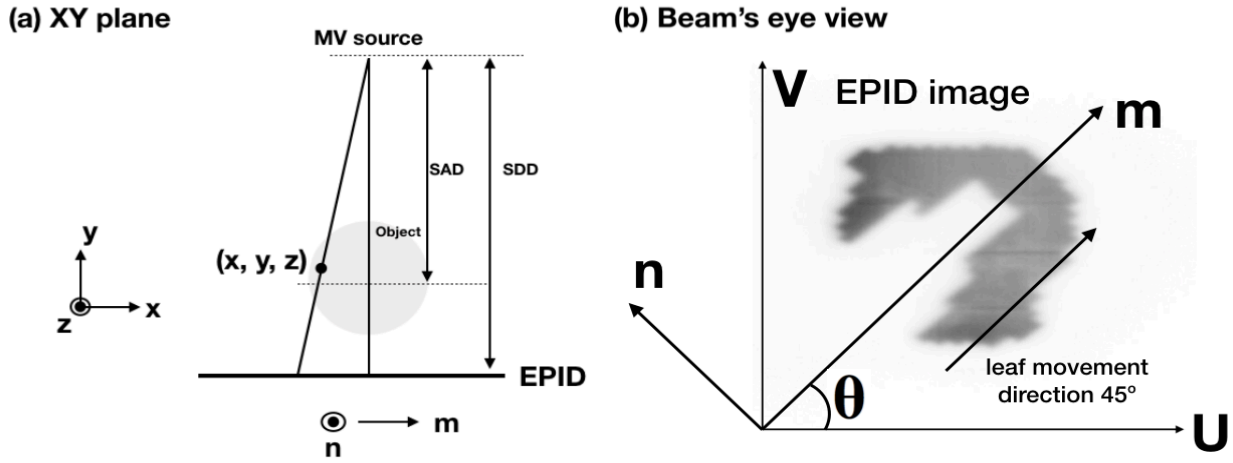


Figure 2.2. Geometry of VMAT-CT reconstruction. (u, v) is the generic EPID image coordinate and is aligned with the panel's edge, while (m, n) is chosen so that m is parallel to MLC leaf movement direction. (a) The X-Y plane when gantry angle is 0°, notice z and n are parallel. (b) A typical beam's eye view. (m, n) is rotated θ degree relative to (u, v) counterclockwise when the collimator angle is θ.

Here we introduce a 3D image rotation after VMAT-CT back-projection at each gantry angle to preserve most of the information on EPID (Figure 2.2.) and then sum all angles' contribution as the final reconstruction:

$$O(x,y,z) = \frac{1}{2}\frac{\Theta(\int_0^{2\pi} T_R M_\beta\left(m',n\right)d\beta-\beta')}{\frac{1}{2\pi}\int_0^{2\pi} T_R M_\beta\left(m',n\right)d\beta}\times$$

$$\int_0^{2\pi} T_R\left[M_\beta(m',n)\int_{-m_{max}}^{m_{max}} dm\, D_k^{extrap}(m,n)e_R(m-m')\right]d\beta \quad (1)$$

where $O$ represents the object, $\beta$ is the gantry angle, $m$ and $n$ are rotated coordinates (Figure 2.2.), $T_R$ is the rotation matrix which is the combination of the rotation around y-axis for $-\theta$ ($\theta$ is the collimator angle), and the rotation around z-axis for $-\beta$ and can be expressed as:

$$T_R = \begin{bmatrix} cos\theta cos\beta & cos\theta sin\beta & -sin\theta \\ -sin\beta & cos\beta & 0 \\ sin\theta cos\beta & sin\theta sin\beta & cos\theta \end{bmatrix} \quad (2)$$

The other parameters were defined in 2010 study (Poludniowski *et al.*, 2010): $M_\beta$ is the masking function which is a measurement of how many rays pass through each calculated voxel, $D_k^{estrap}$ is the extrapolated EPID image for the $k$-th projection, $e_R$ is the local tomography filter, $\Theta$ is the Heaviside step function which eliminates reconstruction points that have too little data available.

Because we are integrating along the direction of MLC movement which is $m$-direction, MLC will not split the beam aperture into more than one connected region in the $u$-direction as shown in Figure 2.2.(b), hence we can preserve more beam information and reduce streaking artifacts.

Compared to the old MLCi2 head, EIPD images obtained on Agility head with the same sampling rate were blurrier due to the faster MLC movement. An erosion with a disk of a radius around 25 pixels was performed on both EPID image and masking function to remove the blurriness, creating lower and upper bounds in each row along m-direction.

Because VMAT-CT does not contain the entire patient anatomy and has no quantitative density information, image registration between VMAT-CT and planning CT was performed. For

rigid phantoms, rigid registrations were performed in MATLAB (MathWorks Inc., Natick, MA) to detect any possible shift or rotation, and planning CT was cropped to a similar region as VMAT-CT for better registration result. During image registration, the planning CT was moving while VMAT-CT was fixed, and the registered set was interpolated to match planning CT's resolution. The original un-cropped planning CT was applied with the same registration matrix to create a so-called "VMAT-CT+" image set in which the planning CT was updated with VMAT-CT's information in local geometry pertaining to the planning target volume (PTV) area. For deformable phantom, deformable registration workflow in MIM (MIM Software Inc., Cleveland, OH) was used. A rigid alignment between the VMAT-CT and the whole planning CT was performed prior to deformable registration and this rigid registration matrix was applied to the whole planning CT. A local deformation was then performed, and local deformable matrix was applied to the local PTV area on the planning CT to generate VMAT-CT+.

2.2.3. Tracking and Art Based on VMAT-CT

We incorporate real-time machine delivery information into dose calculations instead of relying on original treatment plans in TPS. For a full VMAT arc, there are usually around 89 control points in TPS, while there are usually over 250 timestamps recorded in Linac log, which can be considered as over 250 new control points. These new control points recorded by Linac log can be written into the beam delivery file where Pinnacle stores beam information to replace the old control points. The dose calculation was then performed using the new beam delivery file and the new VMAT-CT+ image set.

For rigid phantoms, a shift of 1 cm in X-direction was purposely applied after initial setup to mimic a potential shift of a patient and to test if VMAT-CT can detect the expected shift. Dose calculated on VMAT-CT+ was compared to the original planning dose to find the difference, and

3D gamma (Wendling *et al.*, 2007) was calculated with an acceptance criteria of 3% and 3mm. For these phantoms, since the organs in phantoms were different in shape and density from the real patients, we only tested the accuracy of VMAT-CT reconstruction and the effect of intrafractional shift on dose rather than evaluating the original planning goal like PTV coverage and dose to organs at risk (OARs).

For the deformable lung phantom, we created a customized SBRT plan based on the phantom geometry and optimization goals used for SBRT lung plans in TPS, and made sure the plan was clinically realistic. After CT scan, the phantom was deformed by pulling the string attached to the tumor and remained in the deformed state. CBCT was acquired right before plan delivery and was used as the ground truth ($CBCT_{ground}$) since the phantom could not move on its own and there should not be any geometry difference between VMAT-CT and $CBCT_{ground}$. The reason we did not scan the phantom again with CT after deformation was to eliminate any possible geometry change in the process of moving the phantom from Linac couch to CT scanner. We tracked the geometry change using VMAT-CT+ and calculated the dose PTV received. If the original PTV prescription goal was not met, ART would be performed on VMAT-CT+ image and the VMAT plan would be reoptimized in TPS to meet the prescription dose goal for PTV.

We also compared treatment tracking based on VMAT-CT+ with those based on CBCT because CBCT was used in most ART studies (Li, 2011). CBCT was taken with Elekta XVI prior to beam delivery for phantom setup with a resolution of 1 mm × 1 mm ×1 mm, and CBCT images were exported to Mosaiq and further exported into multiple DICOM files. For rigid phantoms, planning CT was rigidly registered to CBCT in MATLAB and the registered image set has the same resolution as planning CT. Similar to VMAT-CT, we made a 1-cm shift in X-direction after initial setup to mimic a possible patient geometry change during beam delivery. For the deformable

phantoms, planning CT was deformably registered to CBCT in MIM. Similar to VMAT-CT+ images, registered CBCT/planning CT DICOM files and the new beam delivery file incorporating all control points recorded by Linac log were imported into Pinnacle and dose calculations were performed.

### 2.2.4. Patient Study

EPID images of a lung patient treated with VMAT was acquired to test the feasibility of 3D tracking of VMAT based on VMAT-CT. Lung patients whose breathing does not affect the tumor position very much usually do not have 4D CT and are usually treated with 2 half arcs to reduce the dose to the contralateral lung. For those patients, we expect to see the delineation of the boundary between soft tissue and lung or trachea. Similar to the phantom study, patient's CBCT was acquired before treatment, and EPID images were acquired in movie mode during beam delivery. At the same time, Linac log was acquired with Mobius log software (Mobius Medical Systems, Houston, TX). VMAT-CT was reconstructed based on EPID images, and planning CT was registered with VMAT-CT to create VMAT-CT+. New beam delivery file was created with the control points in the Linac log. Dose was calculated with in-treatment geometry information from VMAT-CT+ and also the in-treatment machine information from the new beam delivery file. 3D gamma map between the VMAT-CT based dose was compared to the original planning dose.

Planning CT was also registered to the CBCT to create CBCT+, and dose delivered was calculated on CBCT+ for comparison. 3D gamma map between CBCT based dose was compared to the original planning dose.

### 2.2.5. VMAT-CT Reconstruction Criteria

Not all clinical VMAT plans are suitable for VMAT-CT reconstruction, and we found the plans that could be used for VMAT reconstruction were those planned to deliver dose to a more

regular-shaped and concentric region, i.e. plans that have less information cropped out or blurred by MLC. The masking function defined in Poludniowski *et al.* (2010) is a measure of how many rays passing through the calculated voxel, and the shape of the isodose line would be more concentric if the masking function was more concentric. Another factor is the number of images we can acquire during beam delivery, which is controlled by the dose rate.

### 2.2.6. Uncertainty Analysis

The main uncertainties that may affect the final dose in our study were from rigid or deformable registration.

To evaluate the uncertainties from rigid registrations, a shift of 1 cm was applied to the Rando and Atom phantom in X, Y, and Z directions separately. The differences of the transformation matrix for aligning VMAT-CT and planning CT compared to the 1-cm shift would be the uncertainties. This process was repeated multiple times (different plans) and a mean uncertainty was obtained. The impact of uncertainty from rigid registration on dose was tested by shifting the planning CT the mean uncertainty in each direction separately in a copy of the original plan in TPS and calculating dose difference and 3D gamma compared with planned dose. Since shifting the planning CT is equivalent to shifting the isocenter, we shifted the planning CT by the mean x,y,z uncertainty from rigid registration by shifting the isocenter the exact same distance in opposite direction, and calculated dose. The same dose grid for dose calculation was used before and after the shifts and 3D doses were compared voxel to voxel, and the largest point dose difference was generated. The gamma criteria used is still 3mm and 3%.

To evaluate the uncertainties from deformable registrations, we used the in-house deformable phantom shown in Figure 2.1.. As explained previously, $CBCT_{ground}$ was used as the golden standard after deformation. Gross tumor volume (GTV) on planning CT was contoured by

setting a HU threshold and PTV was expanded from GTV by 5 mm. After registering the moving image (planning CT) with the reference image (VMAT-CT or $CBCT_{ground}$), PTV contour on planning CT was transferred to VMAT-CT+ and $CBCT_{ground}$, and comparison of PTV contour in VMAT-CT to that in $CBCT_{ground}$ can be done by measuring the same contour-based parameters: Hausdorff distance (Jafarinejad-Farsangi *et al.*), mean distance to agreement, dice similarity coefficient (Gradishar *et al.*), and Jaccard coefficient (Brock *et al.*, 2017; Woerner *et al.*, 2017). This process was repeated multiple times (different deformations) and a mean uncertainty was obtained. The impact of uncertainty from deformable registration on dose was tested by expanding or shrinking the PTV isotropically by the average HD in a copy of the original plan in TPS and calculating dose difference and 3D gamma compared with planned dose. Mean PTV dose was compared before and after expansion or shrinkage. The gamma criteria used is 3% and 3mm.

## 2.3. Results

Figure 2.3. . shows typical planning CT, VMAT-CT and VMAT-CT+ images. All VMAT-CT are local to the PTV region and VMAT-CT+ images show the entire FOV. The colors in VMAT-CT+ images in Figure 2.3. are visualization aids and are not used in other figures.

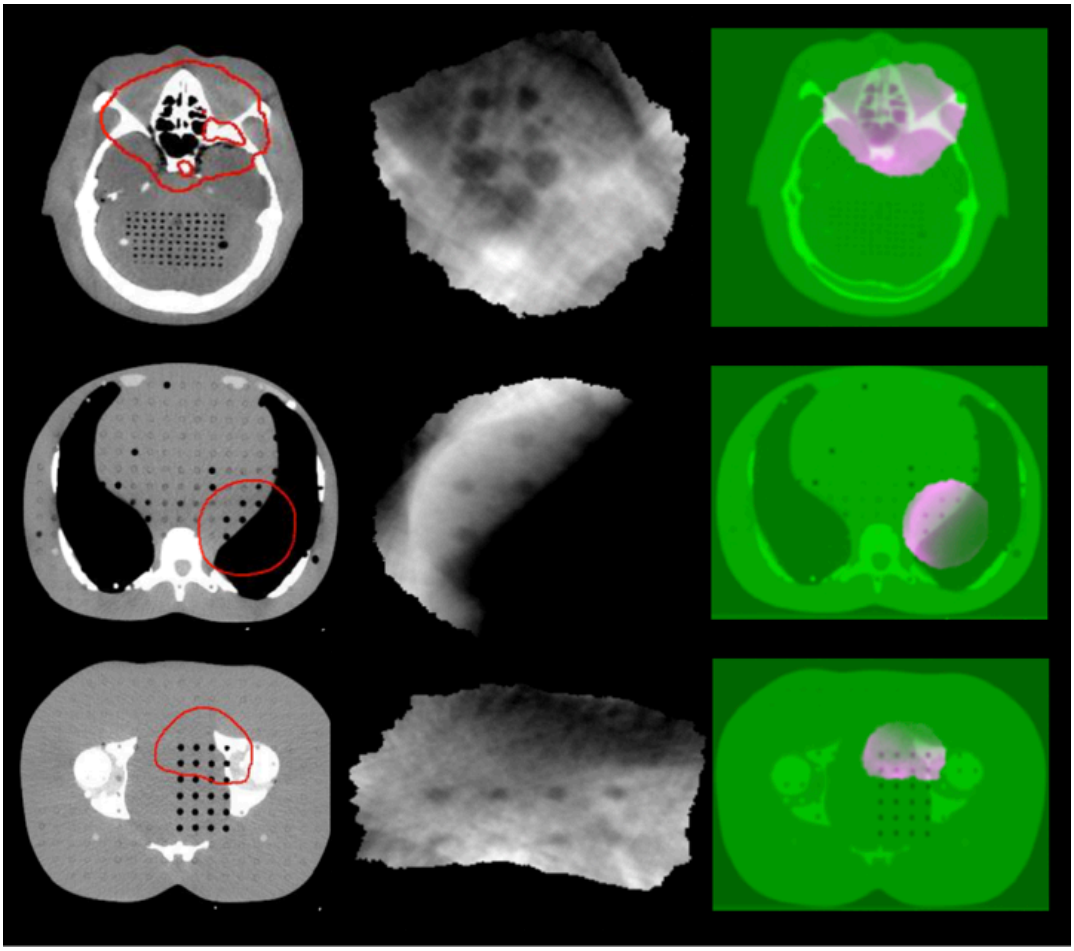

Figure 2.3. Axial view of planning CT images overlaid by the red prescription isodose lines (first column), reconstructed VMAT-CT images (second column), and VMAT-CT+ image sets containing registered VMAT-CT (pink) and planning CT (Green *et al.*) (third column) for a head plan (top row), an abdomen plan (middle row), and a prostate plan (bottom row).

Figure 2.4. shows planned dose calculated on shifted (1 cm) original planning CT (first column), delivered dose calculated on VMAT-CT+ (second column) and on CBCT (fourth column) for the Rando phantom. 3D Gamma plots (passing rate 100% for all plans) of comparison between VMAT-CT+-based dose and planned dose (third column) shows VMAT-CT+ can track the 1-cm shift that we intentionally applied and can be used to calculate the true dose delivered to the phantom. CBCT cannot track any change after initial setup so dose calculated on CBCT does not represent the true delivered dose. The 3D Gamma passing rate for the comparison between CBCT-

based dose and planned dose is 38.83%, 48.23% and 69.97% for brain, abdomen and prostate plans respectively (fifth column). Notice here the 3D gamma plot shows a lot of voxels reaching 10, which is the upper limit set by the searching radius from the evaluated voxel.

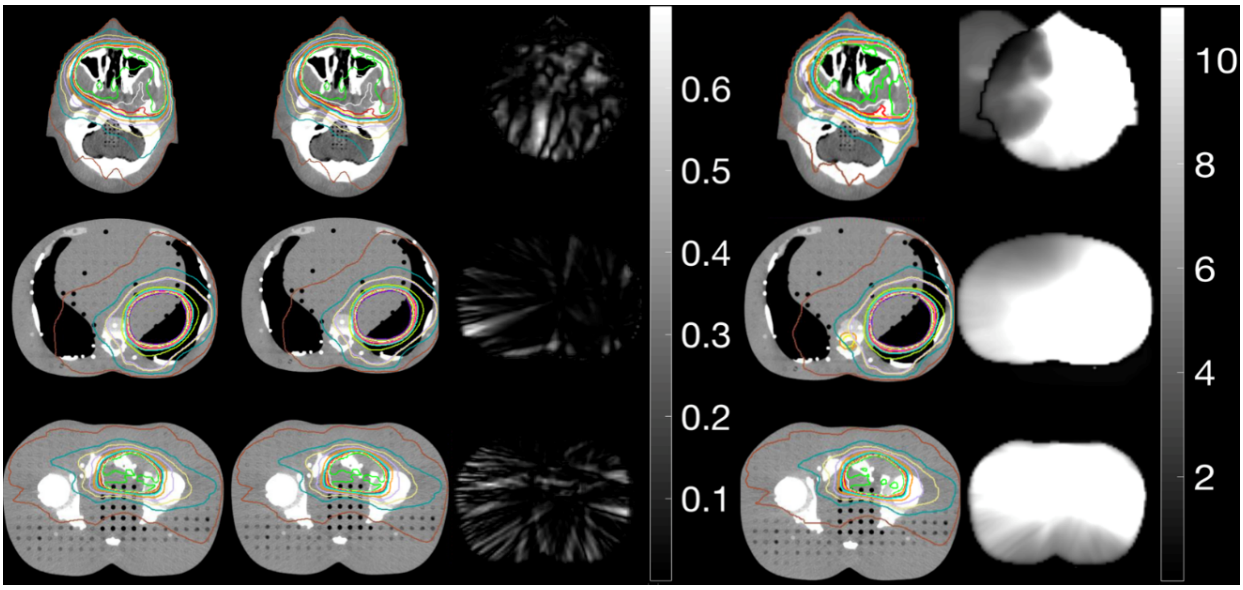


Figure 2.4. Axial view of dose calculated on shifted planning CT (1st column), VMAT-CT+ (2nd column), and CBCT (4th column), and 3D Gamma plot (3rd and 5th columns) (planning CT is used as the reference) for a head plan (top row), an abdomen plan (middle row), and a prostate plan (bottom row).

Figure 2.5.(a) shows the result of deformation and dose calculations for the deformable lung phantom. VMAT-CT can track the phantom deformation correctly compared with ground truth (Gamma passing rate 100%), while pre-treatment CBCT cannot. Figure 2.5.(b) shows the dose volume histogram (DVH) for the original plan, plans after deformation and re-planning. The PTV had 95% coverage of the prescription dose in the original plan, dropped to 92% after phantom deformation but went up to 95% after re-planning. Interestingly, the lung dose went down significantly after ART due to the larger distance between tumor and lung after deformation.

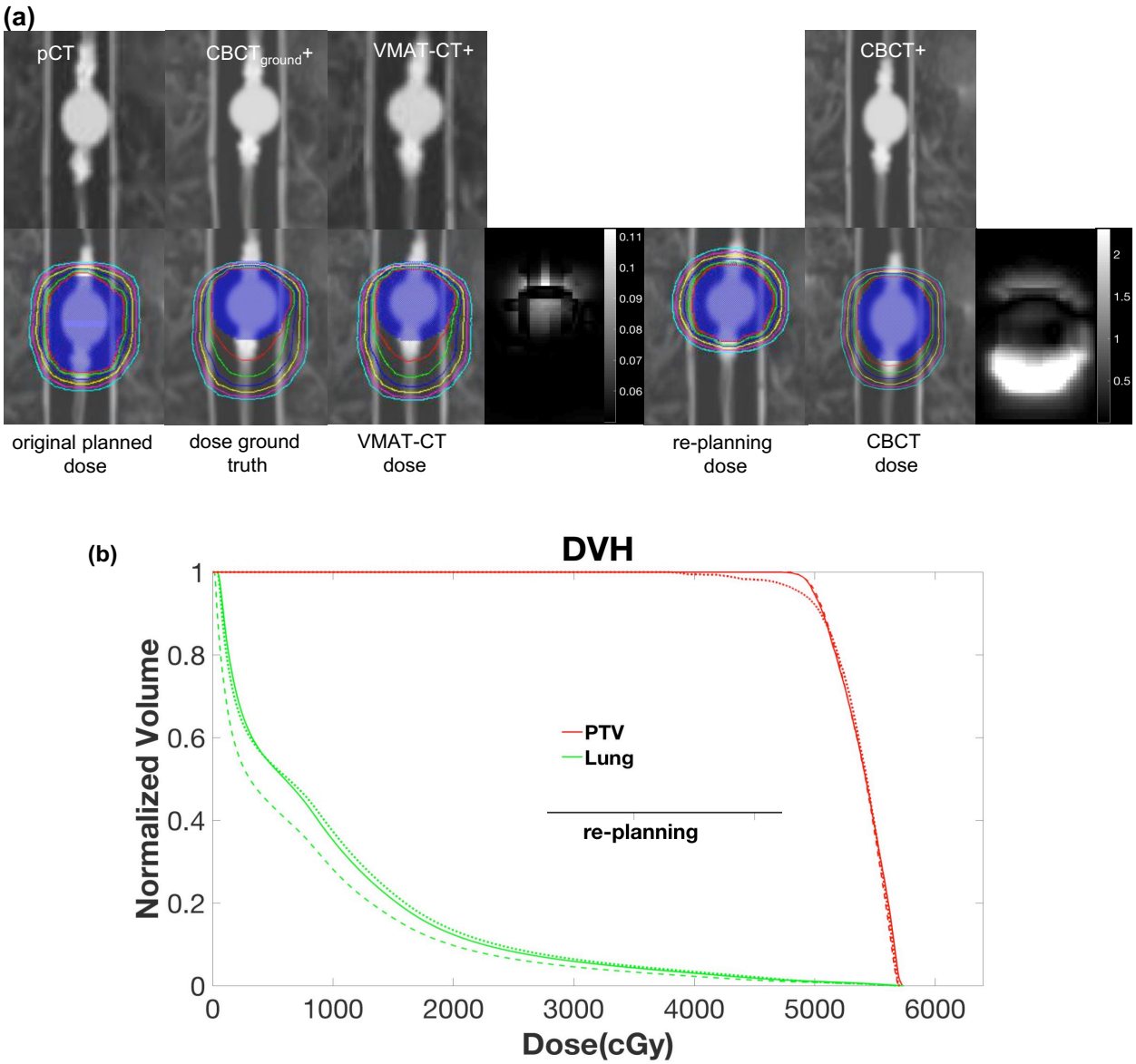


Figure 2.5. Demonstration of ART on deformable phantom. (a) (Top row) comparison of original planning CT (pCT), CBCT$_{ground}$+ (pCT registered to CBCT$_{ground}$), VMAT-CT+, CBCT+ (pCT registered to pre-treatment CBCT); (bottom row) dose distributions in original plan, dose after deformation based on CBCT$_{ground}$, dose after deformation based on VMAT-CT+, 3D Gamma plot of comparison between VMAT-CT dose and dose ground truth, re-optimized dose based on VMAT-CT+, dose based on pre-treatment CBCT, and 3D Gamma plot of comparison between CBCT dose and dose ground truth. The blue shaded area is the original and deformed PTV contour. (b) DVH of original plan, after deformation plan and re-planning plan.

Figure 2.6. shows the result of geometry change and dose calculations for the 3D VMAT lung patient. Since in our clinic, we do not have in-treatment 3D/4D CBCT, the closest verification for patients is pre-treatment 3D CBCT taken on the same day. VMAT-CT can track the patient's geometry change correctly compared to CBCT taken on the same day (Figure 2.6. (a)). In Figure 2.6. (b), the PTV had 98.4% coverage of the prescription dose in the original plan, while the PTV has 99.8% coverage of the prescription dose based on CBCT and VMAT-CT, which indicates no need to re-plan. The 3D gamma passing rate between CBCT based dose to the original planned dose is 99.0%, while the 3D gamma passing rate between VMAT-CT based dose to the original planned dose is 98.6%. The 3D gamma criteria used here is 3mm and 3%.

With different dose rates, the overall reconstruction results were similar. The possible reason is the number of high-quality images did not increase significantly although the total number of images increased. Figure 2.7. shows a typical plan with a masking function that has more than one connected region, and VMAT-CT could not be reconstructed using this plan. It also shows a typical plan that has just one connected region in the masking function and can be reconstructed successfully. The reconstruction criteria can therefore be expressed as: VMAT-CT can be reconstructed based on VMAT plans that have only one connected region in their masking functions; VMAT-CT can show some discernable structures in certain slices or only a section of a slice or cannot be reconstructed at all based on VMAT plans that have more than one connected region in their masking functions; plans that have more projections and bigger MLC openings are inherently easier to reconstruct, e.g. SBRT lung plan in our study has wider MLC openings than other plans and requires much less images to reconstruct.

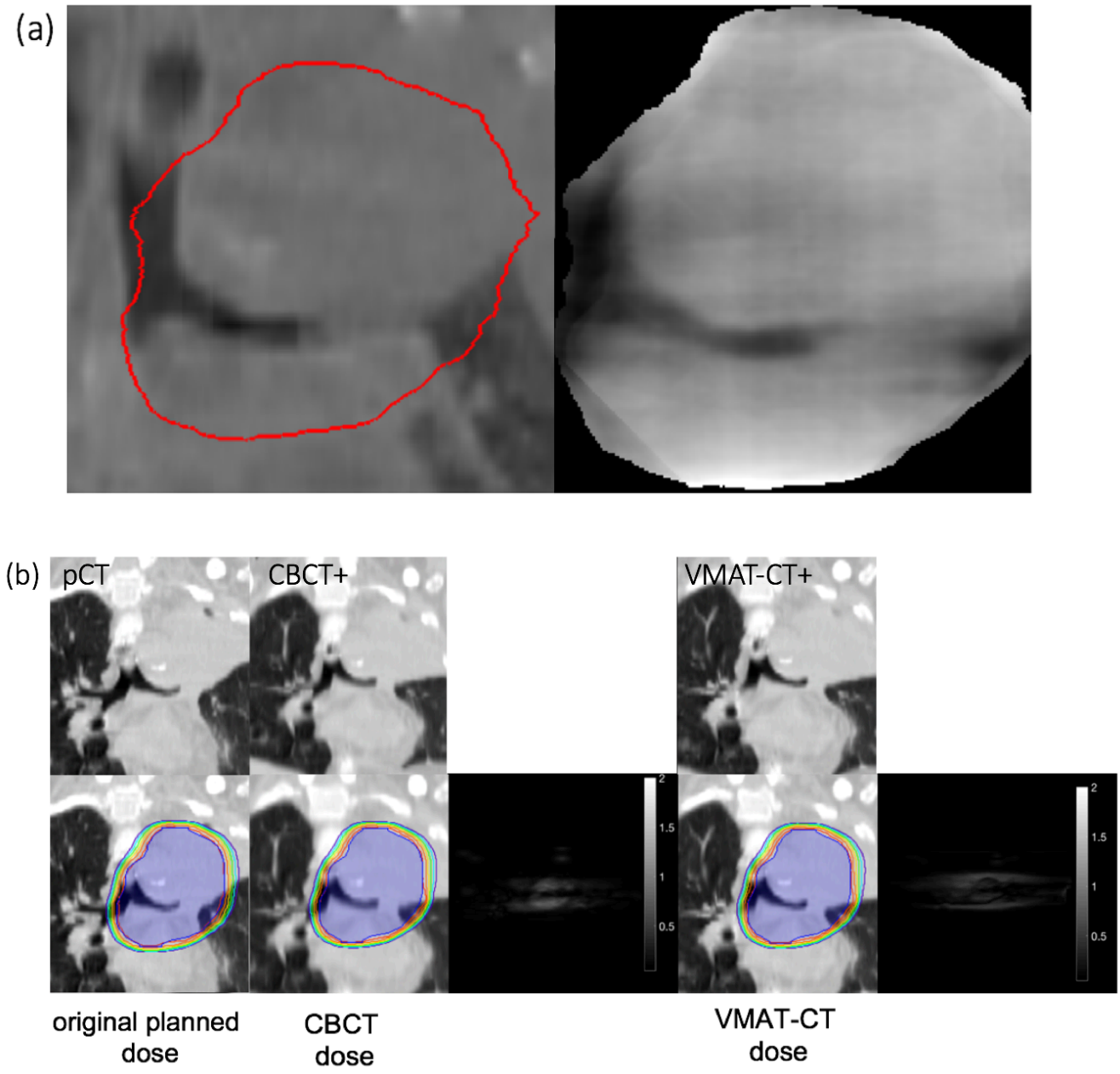


Figure 2.6. Dose comparisons on patient. (a) Comparison of CBCT with VMAT-CT. (b) (Top row) comparison of original planning CT (pCT), CBCT+ (pCT registered to pre-treatment CBCT), VMAT-CT+; (bottom row) dose distributions in original plan, dose based on pre-treatment CBCT, and 3D Gamma plot of comparison between CBCT dose and original planned dose, dose based on in-treatment VMAT-CT+, 3D Gamma plot of comparison between VMAT-CT dose and original planned dose. The blue shaded area is the original and deformed PTV contour.

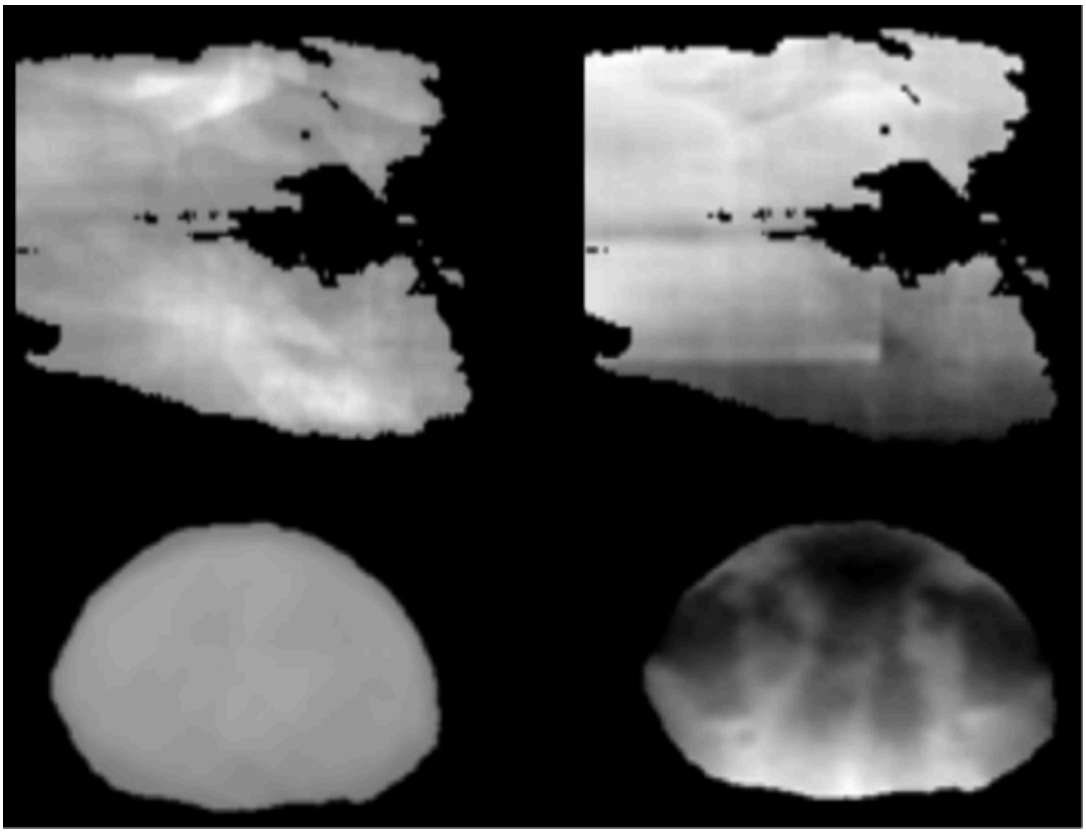

Figure 2.7. Reconstruction criteria. (Top row) a typical clinical plan that cannot be used for VMAT-CT reconstruction, its masking function (top left) and the reconstruction result (top right). (Bottom row) a typical clinical plan that can be used for VMAT-CT reconstruction, its masking function (bottom left) and the reconstruction result (bottom right).

Table 2.1. shows the rigid registration uncertainties when planning CT is registered to VMAT-CT. Table 2.2. shows the deformable registration uncertainties for the lung deformable phantom. The largest potential point dose uncertainty from rigid registration by shifting the planning CT the mean uncertainty in each direction is 0, 0.49 and 2.49 Gy for x, y and z-direction respectively. The 3D gamma passing rate after shifting the planning CT the mean uncertainty in each direction is always 100%. For the deformable registration, the expansion of the mean HD reduces the mean PTV dose by 1.39 Gy while the shrinkage increases the mean PTV by 0.82Gy. The 3D gamma passing rate after expansion or shrinkage is 99.97% and 100% respectively.

Table 2.1. Rigid registration error when planning CT is registered to VMAT-CT. SD: standard deviation.

| Tries | X (mm) | Y (mm) | Z (mm) | Total (mm) |
|---|---|---|---|---|
| 1 | 0.00 | 0.97 | 0.00 | 0.97 |
| 2 | 0.00 | 0.00 | 0.03 | 0.03 |
| 3 | 0.01 | 0.01 | 0.03 | 0.03 |
| 4 | 0.00 | 0.00 | 2.50 | 2.50 |
| Mean | 0.00 | 0.20 | 0.51 | 0.88 |
| SD | 0.01 | 0.48 | 1.24 | 1.17 |

Table 2.2. Deformable registration error when planning CT is registered to VMAT-CT. SD: standard deviation.

| Tries | HD (mm) | MDA (mm) | DSC | Jaccard coefficient |
|---|---|---|---|---|
| 1 | 1.84 | 0.46 | 0.93 | 0.87 |
| 2 | 1.48 | 0.34 | 0.95 | 0.91 |
| 3 | 1.77 | 0.44 | 0.94 | 0.88 |
| 4 | 1.22 | 0.23 | 0.97 | 0.94 |
| Mean | 1.58 | 0.37 | 0.95 | 0.90 |
| SD | 0.29 | 0.11 | 0.02 | 0.03 |

## 2.4. Discussion

We extended the VMAT-CT concept, enlarged the FOV by registering VMAT-CT with planning CT and created VMAT-CT+, evaluated location and dose tracking based on VMAT-CT+, and adapted plan based on VMAT-CT+ when the prescription dose goal was not met. Criteria for VMAT-CT reconstruction and possible uncertainties were also evaluated.

Our study has multiple strengths. First, our VMAT-CT reconstruction is based on the latest Linac MLC and real clinical plans. Poludniowski *et al.* (2010) and Kida *et al.* (2011) were able to reconstruct 3D or 4D local VMAT-CT images. However, their reconstructions were based on plans with slower MLC from the previous generation of Linac head, or with MLC movement constraint to ensure target was always exposed during treatment. With Elekta Versa agility head, fewer EPID images can be collected from each VMAT plan and EPID images can have very blurry edges

because MLCs are thinner and move faster. A lot of the clinical VMAT plans will have heavily truncated beam aperture causing streaking artifacts in VMAT-CT reconstruction. We eroded the edges of these EPID images to remove the blurry area and improved VMAT-CT quality. Second, the collimator angle in our plans is not 0° or 180°, which means the rotation matrix we introduced can apply to real clinical plans and our method has a broader application. For an EPID image in which the beam aperture is disconnected in the horizontal direction due to collimator angle, rotation guarantees all information in the disconnected region projects back therefore preserves the most information, while the traditional methods may lose information, e.g. interpolate between the two regions or simply cut off one section of the disconnected region and only keep the other section. Third, we incorporated real-time machine delivery information into dose calculations. The control points in the recorded machine log is always different from the control points in TPS because the control points are 4 degree apart in TPS but are recorded with an average of 0.2 s apart in the machine log, therefore it is important to consider the possible error during treatment delivery since Linac is delivering the beam the way recorded in the machine log instead of the way in TPS to meet the machine hardware limits like MLC speed, gantry rotation speed, etc. The machine delivery log records the machine parameters every 0~0.6 s with an average of 0.2 s, and it tracks the machine performance very closely and provides information for delivery validation.

Compared with previous tracking based on CBCT, tracking based on VMAT-CT+ shows superior results since VMAT-CT+ can detect phantom/patient geometry change during beam delivery, although the geometry change for real patients after setup may not be as large as 1cm if the treatment site is not susceptible to movement. However, the 1cm shift was applied after CBCT acquisition and before VMAT beam delivery in this study. If the patient has any intra-fraction movement, VMAT-CT would reflect the average result of the overall movement and would have

a blurrier target delineation, which would increase the difficulty for deformable registration. Since VMAT-CT only displays geometry information pertained to the PTV region, if there is a significant amount of geometry change, e.g. significant weight loss, or movement of other parts of body, it would not be identified on the VMAT-CT and CBCT would be very helpful in such situations. Notice the way we evaluated the impact of uncertainty from rigid or deformable registration on dose. These dose uncertainties may not apply to other geometry or plan since it is specific to a given phantom or plan, and we presented them to show typically what the potential dose uncertainty could be.

The limitation of this study is image quality. One possible improvement could be the sampling rate of acquisition of EPID images. The sampling rate in this study, which is the sampling rate of Elekta Versa, was 4 frames per second. Considering MLCs in the new model of Linac head are moving faster, the projection images will be less blurry and more high-quality images can be collected with faster sampling rate and therefore reconstruction image quality can be improved. In the future, iterative reconstruction methods can also be explored to compensate for less information provided the same machine parameters.

## 2.5. Conclusion

VMAT-CT was reconstructed under more stringent conditions, dose was calculated with in-treatment geometry, and ART was carried out when prescription dose was not met. Overall VMAT-CT can be a very promising tool for patient positioning, tumor targeting, normal tissue sparing and treatment QA without introducing any extra dose.

# 3. FEASIBILITY OF 4D TRACKING AND ADAPTATION OF VMAT BASED ON VMAT-CT

## 3.1. Introduction

Stereotactic body radiotherapy (SBRT) has been successfully used to treat sites involving breathing movement like lung and upper abdomen (Heinzerling *et al.*, 2008; Prevost *et al.*, 2008; Ricardi *et al.*, 2015; Herbert *et al.*, 2013) when surgery is not an option. Since SBRT is a hypo-fractional treatment, and organ motion for tumors located close to the diaphragm can be greater than 2 cm (Sonke and Belderbos, 2010), dosimetric errors occur in one fraction can have a significant impact and it is very important to track the location and dose delivered during treatment. Accompanying SBRT, in-treatment four-dimensional (4D) kilovoltage (kV) cone beam computed tomography (CBCT) images can be acquired for position verification (Kida *et al.*, 2012). However, 4D CBCT introduces more extra dose to the patient (Cooper *et al.*, 2019b), and many linear accelerators (Linacs) do not have 4D CBCT option during beam delivery. Usually a 4D or a three-dimensional (3D) CBCT before each treatment fraction is acquired, which does not track tumor location after patient setup or during beam delivery.

Among various radiotherapy techniques, volumetric modulated arc therapy (VMAT) is considered the best way to deliver SBRT because of its short treatment time (Sapkaroski *et al.*, 2015; McGrath *et al.*, 2010). Kida *et al.* (Kida *et al.*, 2011) developed a 4D version of volumetric modulated arc therapy – computed tomography (VMAT-CT) following the concept of VMAT-CT proposed by Poludniowski *et al.* (2010). They compared two tracking methods that were based on 4D VMAT-CT and in-treatment kV CBCT for two patients, and a constraint on MLC motion of 0.1 cm/degree was applied to ensure target was always exposed during treatment, which is not clinically realistic. Reconstruction of 4D VMAT-CT would decrease imaging dose since the images come directly from the treatment beam, provide real-time patient information during the

treatment and allow for treatment tracking. However, there are still some shortcomings of 4D VMAT-CT like limited field of view (FOV) and no electron density information. In addition, adaptive therapy (ART) based on 4D VMAT-CT has not been demonstrated.

We previously reported the feasibility of three-dimensional (3D) tracking and ART based on VMAT-CT (Zhao and Zhang, 2020). The goal of this study is to extend our previous study and develop a technique to track and adapt 4D SBRT treatment based on 4D VMAT-CT. Comparison with tracking based on 4D CBCT and uncertainties associated with 4D VMAT-CT were also evaluated.

## 3.2. Methods and Materials

### 3.2.1. Phantoms, Treatment Planning, and Data Collection

A QUASAR™ programmable respiratory motion phantom (Modus Medical Devices Inc., London, Ontario, Canada) was used in this study (Figure 3.1.(a)). The phantom has an acrylic body and a motor driving a cedar wood cylinder mimicking movement of the lung. The cedar wood cylinder splits in the middle and has a 3-cm diameter ball mimicking a tumor. Another cedar wood cylinder that has a hole to hold an ion chamber inside was also used in this study. We set up the QUASAR phantom to have 2 breathing patterns: one regular sine wave with a period of 4 s and amplitude of 10 mm, and four irregular breathing patterns extracted from a real patient's breathing signal. An in-house deformable lung phantom that was driven by the Quasar phantom was also created for this study, and a schematic figure is shown in Figure 3.1.(b): the sponge inside the latex enclosure represented lungs, a small balloon filled with gel represented the deformable tumor, and the rest of the phantom was filled with rice powder to represent tissue. The deformable tumor was

tied with strings on both sides: one side of it was fixed and the other side was attached to the Quasar phantom to drive the tumor with desired breathing pattern and to deform the tumor.

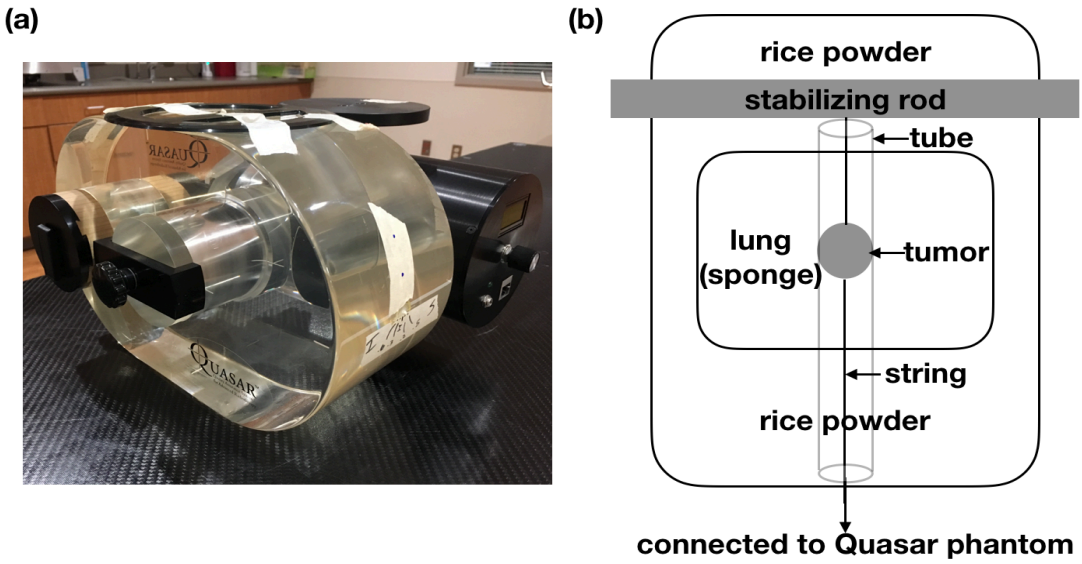


Figure 3.1. (a) Quasar phantom; (b) Descriptive figure of in-house deformable phantom shown.

4D cine planning CT of the QUASAR phantom and the deformable phantom were acquired with a 16-slice GE LightSpeed CT scanner (GE Medical Systems, Milwaukee, WI, USA) and reconstructed with Advantage 4D (GE Healthcare, Waukesha, WI, USA). While acquiring 4D planning CT, a respiratory signal was acquired by the Real-Time Position Management (RPM) Respiratory Gating system (Varian Medical Systems, Palo Alto, CA, USA) concurrently, and a PDF (probability density function) of tumor position versus time was obtained. The gross tumor volume (GTV) was delineated on all 4 phases of 4D planning CT by setting a HU (Hounsfield unit) threshold. Mean position of the PDF was calculated, and from the four phase planning CT data sets, one phase's data set was chosen as the mean position planning CT (MPPCT) if that phase's GTV was closest to the mean position (Harsolia *et al.*, 2008).

4D union and 4D ART plans similar to techniques proposed by Harsolia *et al.* (2008) were created for both QUASAR phantom and the deformable phantom in Pinnacle v9.10 treatment

planning system (TPS) (Philips Medical Systems, Fitchburg, WI, USA). Plans had 6 MV beam and 50 Gy prescription dose which is the standard prescription for SBRT lung cases in our center, and were delivered by Elekta Versa Linac (Elekta Oncology Systems, Crawley, UK). The reason to create 4D union plan is because it is the standard practice for lung SBRT in our clinic. The reason to create 4D ART plans is because Harsolia *et al.* (2008) reported ART can significantly decrease PTV volume and dose to normal tissues and allow for dose escalation, and we want to investigate if VMAT-CT can provide sufficient image information for adaptive correction. For the QUASAR phantom, treatment plans were created with the ball insert. 4D union plans required the contour of the maximum intensity projection (MIP) of the target as GTV, which encompassed all possible locations of the tumor. The GTV was then expanded with a margin to PTV to accounted for microscopic disease and setup error. For 4D ART plans, mean position GTV in MPPCT was expanded by 0.5cm as the CTV and a static plan was generated first based on mean position CTV. The static dose was then convolved with the PDF obtained from 4D cine planning CT to determine the effect of respiratory motion and setup variability, and to find out the necessary margin (CTV to PTV) to ensure the target would receive 95% prescription dose coverage.

3.2.2. Respiratory Signal Extraction and 4D VMAT-CT Reconstruction

Normalized cross correlation (NCC) method used in Kida *et al.* (Kida *et al.*, 2011) was also used in this study to extract respiratory signals from EPID images acquired during VMAT. Without any external surrogates for tumor motion, shifts of tumor between two consecutive EPID images were quantified by computing the NCC matrices of the same fixed area in the two EPID images. The resulting NCC matrix contained the correlation coefficients, and the shift of the tumor (confined to SI direction) correlated to the row number of the maximum value in NCC. Repeating the process for all acquired images and matching the timestamp of EPID images stored in the

iView system, a temporal tumor shift signal was acquired. However, this signal may contain errors brought by gantry rotation that needed to be removed by applying a band pass filter, and 0.2Hz and 1Hz were used as thresholds in this study because patient breathing period is usually between 1s and 5s (Kida *et al.*, 2011). In addition, unlike the plans in Kida *et al.* (Kida *et al.*, 2011), target exposure was not guaranteed during the entire treatment because we did not set any constraint on MLC motion, which is the case for almost all clinical patients, and part of the respiratory signal could be missing. Since the frequencies of the abnormal noise like lost signal (low frequency) and gantry rotation (low frequency) would be eliminated in frequency domain after applying the band pass filter, lost signals would be filled in and the effect of gantry rotation would be eliminated after Fourier transform. This method worked for most breathing patterns, but did not work if the real signal has a drastically different period or amplitude from rest of the signal because the filled signal is an educated guess based on the other parts of the breathing signal. To split the images into 4 phases, a time-based sorting method was used to get approximately same number of images in each phase in order to ensure image quality was comparable in each phase. VMAT-CT reconstruction was then carried out in each phase using the method reported by our group previously (Zhao and Zhang, 2020).

For the QUASAR phantom, rigid registration was performed between 4D VMAT-CT and planning CT since there was no deformable movement. The registration is only performed in the cylinder region where the phantom is moving, not everywhere else since the rest of phantom is static. Because the target was blurred out in 3D free breathing planning CT, we registered the VMAT-CT to the MPPCT where the target was clearly delineated. There are several advantages in choosing MPPCT: (1) we need to register reconstructed VMAT-CT in each phase to images with a clearly delineated contour of GTV; (2) a 3D static dose needs to be calculated on MPPCT

in ART plan (Harsolia *et al.*, 2008); (3) we need to register four phases' doses back to the MPPCT to compose a composite dose which could be overlaid on a clear contour. After one phase's VMAT-CT was rigidly registered to MPPCT, the rigid registration matrix was applied to the moving cylinder insert in MPPCT and pixel-to-pixel electron density propagation was performed between registered region of MPPCT and VMAT-CT to create a fusion image named "VMAT-CT+" in each phase. VMAT-CT+ includes patient position information during the treatment and has the same FOV and Hounsfield Unit (HU) scale as planning CT.

For the deformable phantom, deformable registration workflow in MIM (MIM Software Inc., Cleveland, OH) was used. First, a rigid alignment between each phase of VMAT-CT (primary dataset) and the MPPCT (secondary dataset) was performed, and the rigid transformation matrix was first applied to the MPPCT. A local deformation was then performed and local deformable matrix was applied to the local PTV area on the MPPCT to generate VMAT-CT+ in each phase.

3.2.3. Tracking and Art Based on 4D VMAT-CT

Figure 3.2. shows the workflow of 4D dose reconstruction. Linac log and EPID images were individually time stamped and were synchronized by matching the MLC positions.

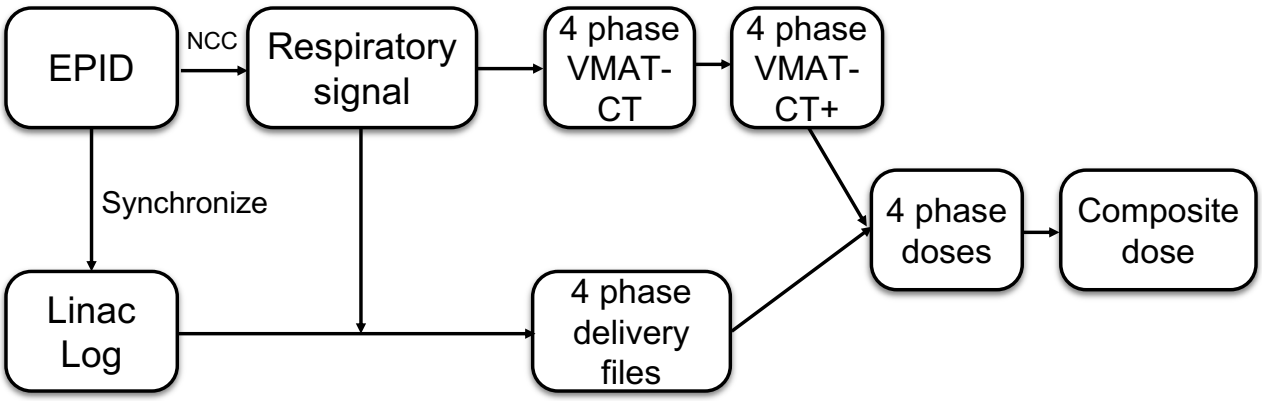


Figure 3.2. Workflow of 4D dose reconstruction based on VMAT-CT+.

The phase-dividing timestamps in EPID images were applied to the Linac log to sort the MLC control points into four phases. Interpolation between control points was performed if any EPID timestamp fell between two control points' timestamps in Linac log (Poulsen *et al.*, 2012) (Figure 3.3.(a)). However, if the respiratory signal was not extracted from EPID images but rather from pre-treatment CBCT images, the respiratory signal was not an accurate representation of the breathing motion during beam-on time. Therefore, in the case of sorting out Linac log control points in 4 phases by evenly dividing the timeline by ¼ of the average period extracted from CBCT, there could be a control point and phase mismatch as shown in Figure 3.3.(b). Four new beam delivery files were generated based on four phases' control points and imported into TPS as described in our previous study (Zhao and Zhang, 2020). Meanwhile four sets of VMAT-CT+ DICOM images were generated and imported back into TPS. Dose was calculated in each phase on its corresponding VMAT-CT+, and each phases' dose matrix was registered using the transformation matrix derived from its VMAT-CT+'s registration to MPPCT. Re-optimization was done when prescription dose for PTV was not met.

For lung patients, certain centers take 4D CBCT before each fraction, and ART has been based on the CBCT images (Sonke and Belderbos, 2010). We therefore evaluated the dose reconstruction differences based on 4D CBCT and 4D VMAT-CT+ under regular and irregular breathing patterns. Before beam delivery, 4D CBCTs of the QUASAR phantom with the ion chamber insert and the deformable phantom were obtained. We extracted the respiratory signal from 4D CBCT projection images using NCC method the same way as we processed EPID images, and both 4D CBCT and Linac log were sorted into 4 phases. MPPCT was registered to each phase of 4D CBCT, dose was calculated in each phase and registered back to the MPPCT using the registration matrix of each phases' image set, and a composite dose was acquired. For both

QUASAR and deformable phantoms, different breathing patterns were used before and after the beam started to mimic a potential change of breathing pattern for a patient.

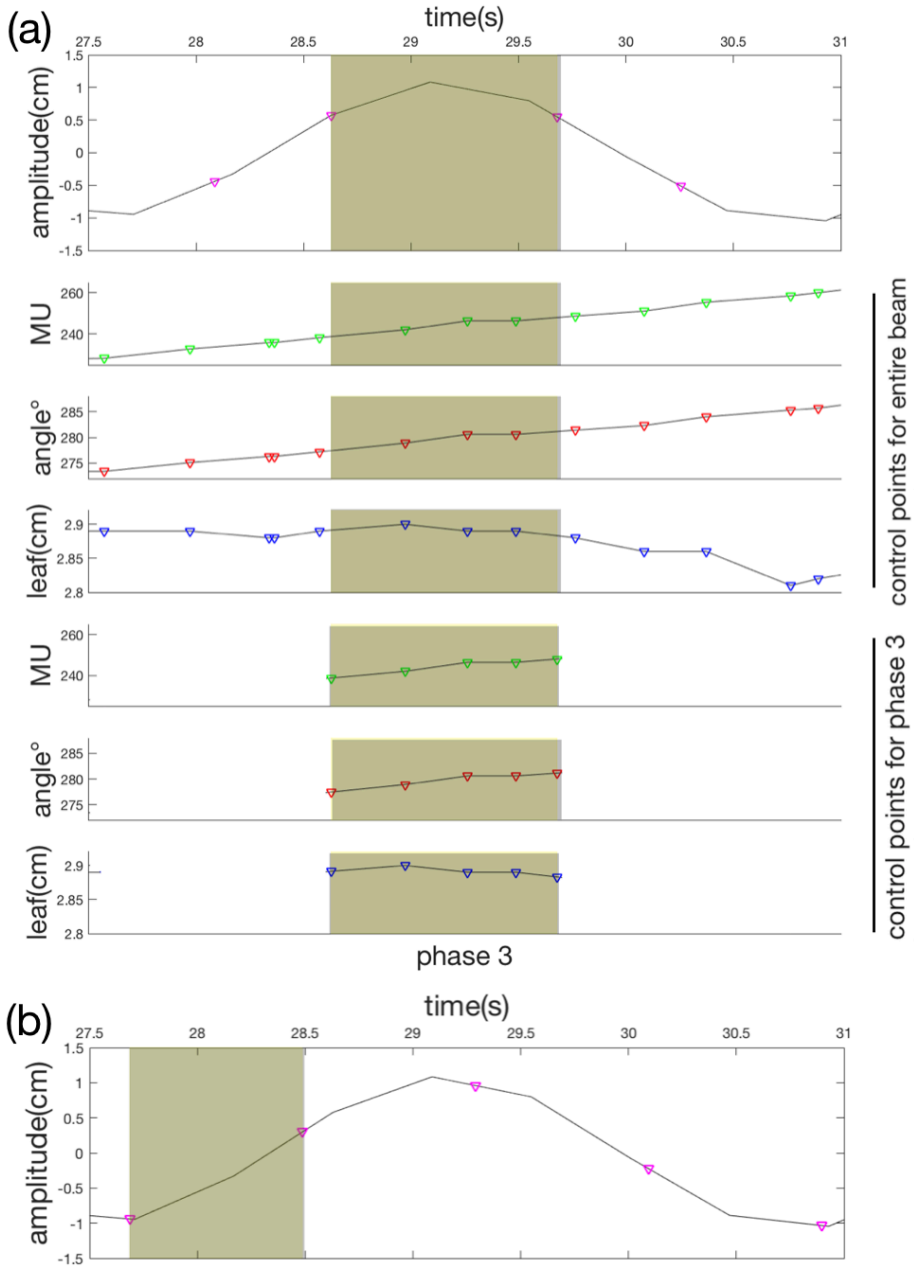


Figure 3.3. Sorting of control points. (a) Interpolation of control points at phase dividing timestamps and sorting of control points into four phases (phase 3 was shown here as an example) when using EPID images during beam delivery to trace respiratory signal; (b) possible mismatch between phase sorting and actual target position when using CBCT before delivery to trace respiratory signal.

Since we don't have in-treatment 4D CBCT in our clinic, ion chamber measurements were performed to verify the accuracy of 4D dose reconstruction for the Quasar phantom. The cedar wood cylinder that can hold an ion chamber and a 0.125cc ion chamber (TN31011, PTW-Freiburg) were used. Active region of the ion chamber was contoured in the MPPCT and dose inside the active region of the ion chamber was averaged to be considered as a point dose. The 4D union and ART plans were copied onto the ion chamber image set and iso-center was placed close to the ion chamber. The couch was moved in the longitudinal direction in intervals of 0.5 cm to measure multiple single point doses. Figure 3.4. shows the ion chamber measurement setup.

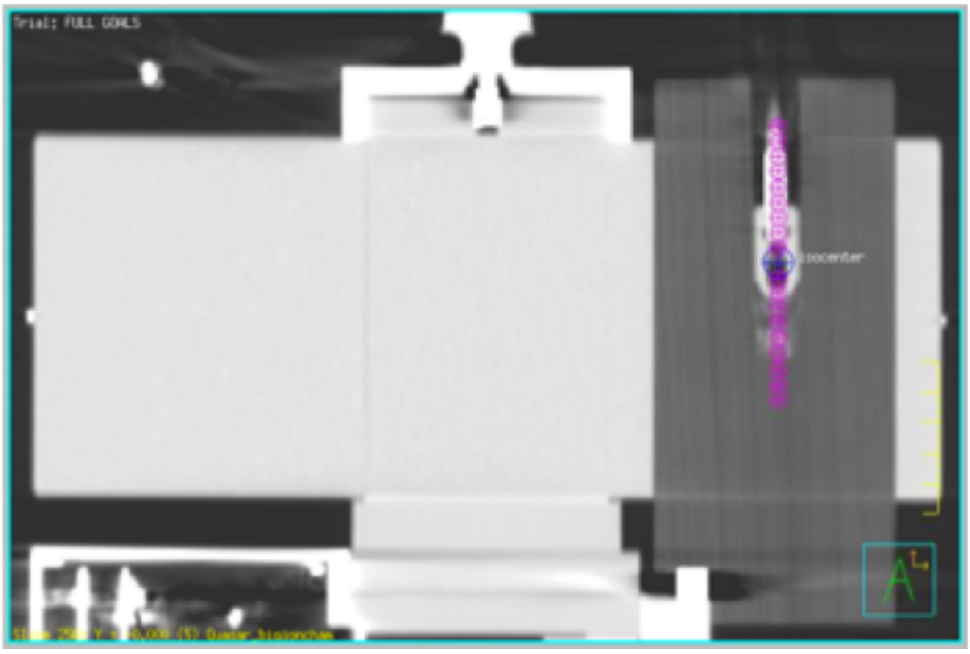

Figure 3.4. Setup for ion chamber measurements. The blue point is the isocenter, and the purple points are ion chamber measurement positions (0.5cm apart along SI direction) for 4D Union plan and offline ART plan.

Ion chamber measurements were compared with point doses calculated in different situations to find out the most accurate way of calculating dose when respiratory motion was present: (1) original planning dose calculated on MPPCT; (2) 4D dose calculated on 4D VMAT-

CT+; and (3) 4D dose calculated on 4D CBCT. After acquiring the dose matrix on the images in each situation, contour of the active region of the ion chamber was shifted by the corresponding distance the ion chamber moved during measurements. There are four different setups: (1) a regular sine wave was fed to the QUASAR phantom during 4D CBCT acquisition, and another regular sine wave with the same amplitude and period but a different initial phase was fed to the ion chamber during beam delivery, and the plan delivered is the 4D Union plan; (2) similar breathing patterns as those used in (1), and the plan delivered is the 4D Adaptive plan; (3) an irregular breathing pattern extracted from a patient was fed to the QUASAR phantom during 4D CBCT acquisition, and another irregular breathing pattern extracted from another patient with different amplitude, different period, different baseline was fed to the QUASAR phantom during beam delivery, and the plan delivered is the 4D Union plan; (4) similar breathing patterns as those used in (3), and the plan delivered is the 4D Adaptive plan. In each of these four different breathing pattern setups, dose calculated on 4D CBCT and 4D VMAT-CT was compared to ion chamber measurements to see if 4D VMAT-CT show superior 4D dose reconstruction accuracy than 4D CBCT.

As for dose verification for the deformable phantom, we acquired 4D CBCT again prior to beam delivery under the same breathing pattern as the pattern would be used during beam delivery. We used this set of 4D CBCT as the ground truth (4D $CBCT_{ground}$) because our deformable phantom cannot hold an ion chamber. By using 4D $CBCT_{ground}$ instead of 4D cine CT, we eliminated the potential geometrical change in the process of carrying the phantom from CT couch to treatment couch. The only drawback of using 4D $CBCT_{ground}$ as the reference is that it did not eliminate potential dose error brought by synchronization of the treatment machine and the breathing pattern extracted from CBCT images: the respiratory signal acquired from CBCT was

before treatment after all and it can only be very close to the respiratory signal during beam delivery. Even if we started the movement of the QUASAR Platform the same time as kV x-ray started, this procedure was still manual and the time for the machine to actually start delivering kV beam could vary every time.

### 3.2.4. Patient Study

EPID images of a lung patient treated with SBRT was acquired to test the feasibility of 4D tracking of VMAT based on VMAT-CT. In our center, patients do not typically receive a 4D CBCT before treatment. Therefore, we did not compare our 4D VMAT-CT based dose to the 3D CBCT. However, we did compare our 4D VMAT-CT to the 4D planning CT. We also compared 4D VMAT-CT based dose to the original planning dose.

After patient setup, EPID images were acquired in movie mode during beam delivery. At the same time, Linac log was acquired with Mobius log software (Mobius Medical Systems, Houston, TX). Respiratory signal was extracted from the EPID images. EPID images and Linac log were synchronized by matching the MLC shape. Then respiratory signal was used to sort both the EPID images and the Linac log into four phases. 4D VMAT-CT was reconstructed by using EPID images in each phase. Then planning CT was registered to the VMAT-CT in each phase to create 4D VMAT-CT+. Dose was calculated in each phase, and four phases' doses were deformably registered to the mean position of the 4D VMAT-CT+ to generate the composite dose. 3D gamma map between the 4D VMAT-CT based dose was compared to the original planning dose.

### 3.2.5. Uncertainty Analysis

To evaluate the uncertainties brought by rigid registrations in 4D cases, we compared the reconstruction matrix between each phase of VMAT-CT and MPPCT with that between each

phase of cine CT and MPPCT under the same breathing pattern for the QUASAR phantom. The impact of uncertainty from rigid registration on dose was tested by shifting MPPCT the average uncertainty in each of X, Y, and Z direction in a copy of the original MPPCT plan to find out the upper point dose difference limit. Similarly to the uncertainty analysis in chap 2, we shifted the planning CT by the mean x,y,z uncertainty from rigid registration by shifting the isocenter the exact same distance in opposite direction, then calculated dose. The same dose grid for dose calculation was used and 3D dose was compared voxel to voxel, and the largest point dose difference was generated. 3D gamma (Wendling *et al.*, 2007) was also calculated with an acceptance criteria of 3% and 3mm.

To evaluate the uncertainty brought by deformable registrations in 4D cases, we used 4D $CBCT_{ground}$ as the geometry golden standard, as we explained in the previous section. In phase-to-phase registration between VMAT-CT+ and MPPCT and between $CBCT_{ground}$ and MPPCT, GTV and PTV was contoured in MPPCT, and transferred to VMAT-CT and $CBCT_{ground}$ thought deformable registration. Deformed GTV and PTV from deformable registration between VMAT-CT to MPPCT was compared to its corresponding phases' GTV and PTV contour in $CBCT_{ground}$, and Hausdorff distance (Sterpetti *et al.*, 2019), Mean distance to agreement (Cebi *et al.*, 2018), Dice similarity coefficient and Jacobian determinant (Brock *et al.*, 2017; Woerner *et al.*, 2017) were evaluated. The impact of uncertainty from deformable registration on dose was tested by expanding or shrinking the GTV contour in each phase of VMAT-CT+ by mean HD, calculating the dose under the same beam delivery file in each phase, and registering back to MPPCT to get a new composite dose. Mean dose of the PTV was evaluated before and after expansion or shrinkage. 3D Gamma was also calculated. The criteria used is still 3% and 3mm.

## 3.3. Results

We verified both regular and irregular respiratory signals extracted from EPID images by comparing them with the input signals fed to the Quasar phantom (Figure 3.5.): for regular breathing pattern, the setup period was 4s and measured period was 3.99s; for irregular breathing pattern, the setup period was 2.66s and measured period was 2.68s.

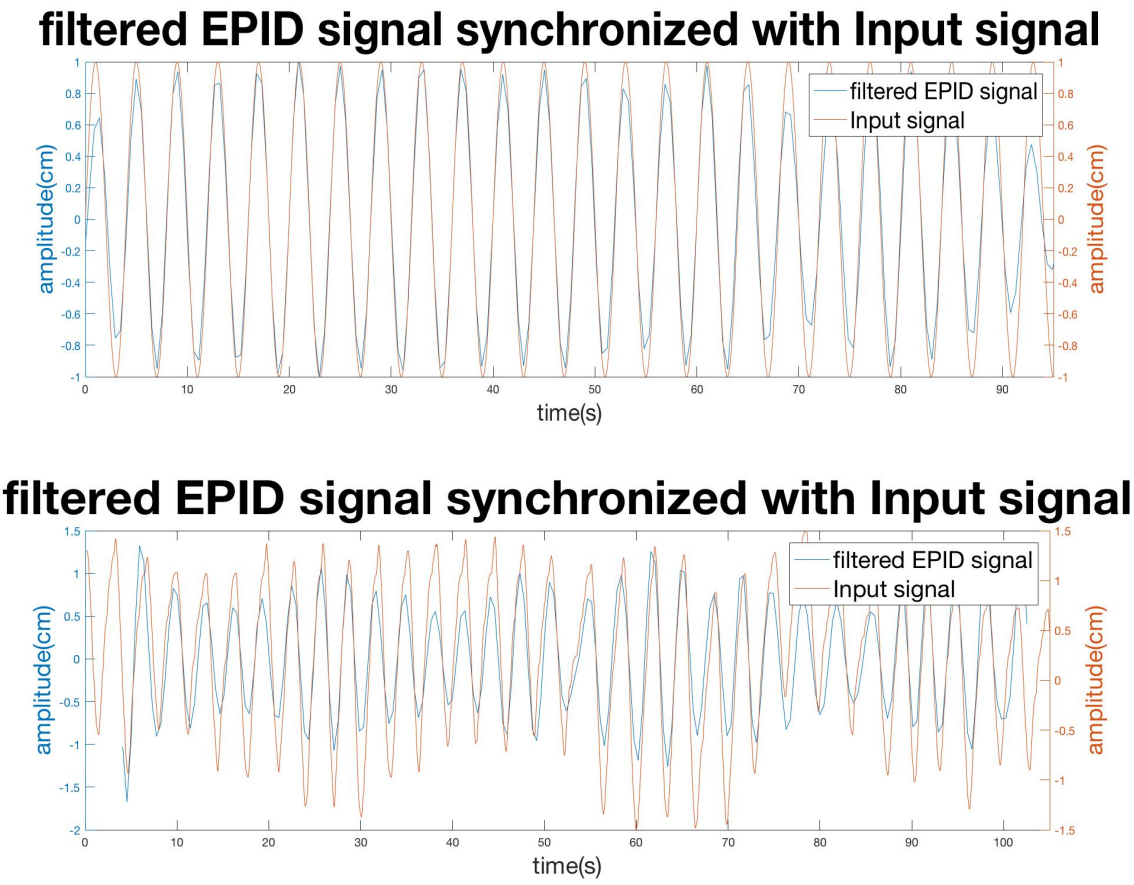


Figure 3.5. Respiratory signals extracted from EPID images were synchronized with input signals to Quasar phantom. Top: regular sine wave breathing pattern. Bottom: irregular breathing pattern.

Note the synchronization is for period, not amplitude. The reason why we did not need to capture the right amplitude is that we sorted EPID images into 4 phases based one time. As long as we captured the right direction of tumor movement, i.e., period or frequency, we can find the correct timestamp of the peaks, which resulted in correct phase-dividing timestamps. Once the

images were sorted correctly, the reconstruction was only dependent on the selected images in that phase and did not reply on the amplitude of the respiratory signal. Locations of center of mass in phases 1 and 3 in VMAT-CT images (Figure 3.6.) were compared with 4D Cine planning CT: for regular breathing pattern, Cine planning CT showed 20mm displacement while VMAT-CT showed 21mm; for irregular breathing pattern, both Cine planning CT and VMAT-CT showed 16mm displacement.

Figure 3.7. compares point dose values based on ion chamber measurements (ground truth) with point doses based on VMAT-CT and CBCT. Dose calculations based on VMAT-CT agree with ion chamber measurements well, while dose based on CBCT do not. For the regular breathing pattern, the two signals fed to the Quasar phantom before and during beam delivery have the same period and amplitude, but they differ in the initial phase shift so the phase sorting based on CBCT would be mismatched to the control points. For irregular breathing pattern, two totally different irregular breathing patterns were fed to the Quasar phantom before and after beam on. For dose based on VMAT-CT, the dose fall-off compared to planned dose (MPPCT) at the shoulder of the dose profile is about 5 mm for the regular breathing pattern and around 4 mm for the irregular breathing pattern at the prescribed dose level (50 Gy). For dose based on CBCT, the dose fall-off is about 5 mm for the regular breathing pattern and around 6-9 mm for the irregular breathing pattern at the prescribed dose level.

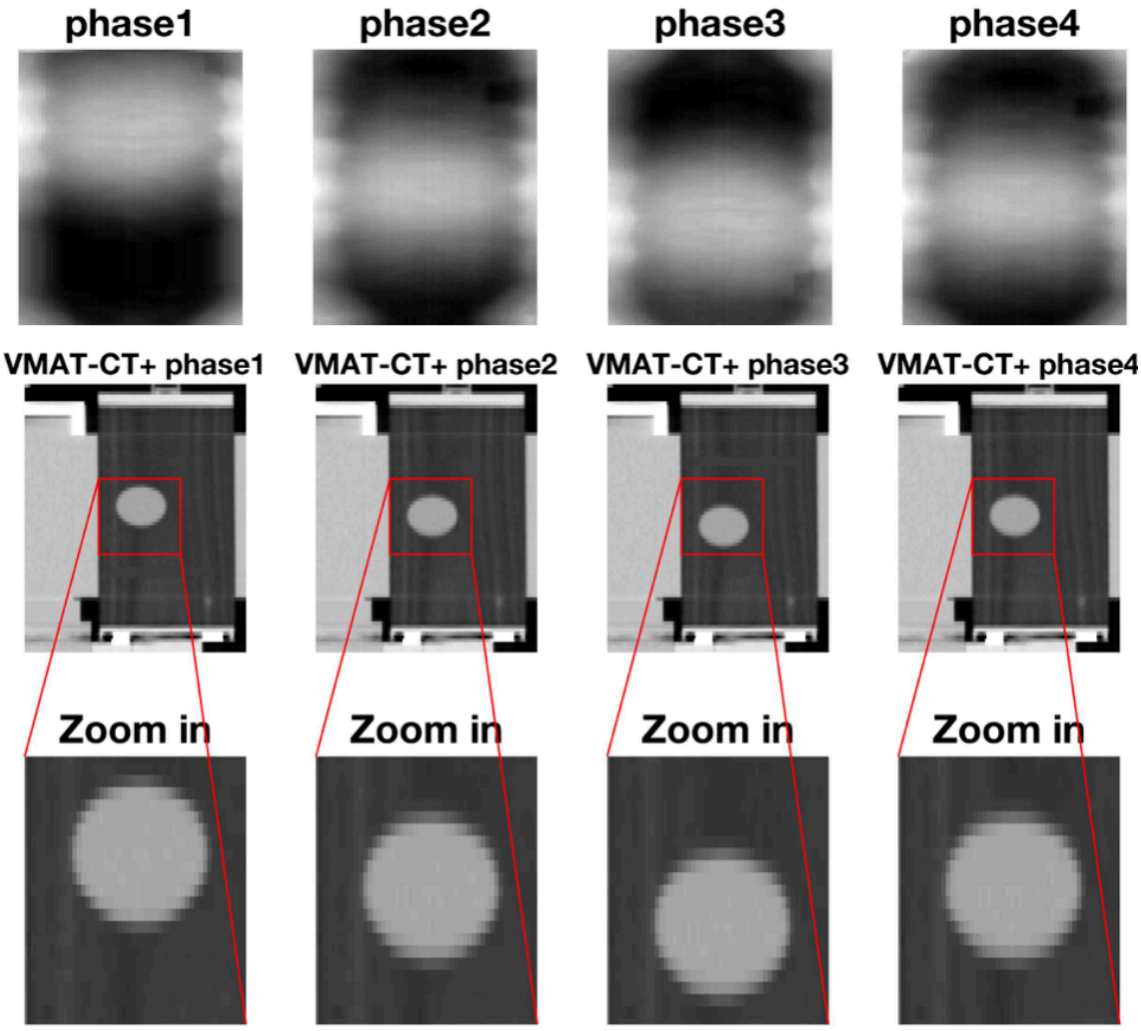


Figure 3.6. Reconstructed VMAT-CT (Premo *et al.*) and VMAT-CT+ (middle and bottom) of the Quasar phantom with a ball insert. The ball was at the peaks at phase 1 and phase 3 and was in the middle at phase 2 and phase 4. This is a reconstruction of 4D union plan based on irregular breathing pattern and time-based phase sorting method.

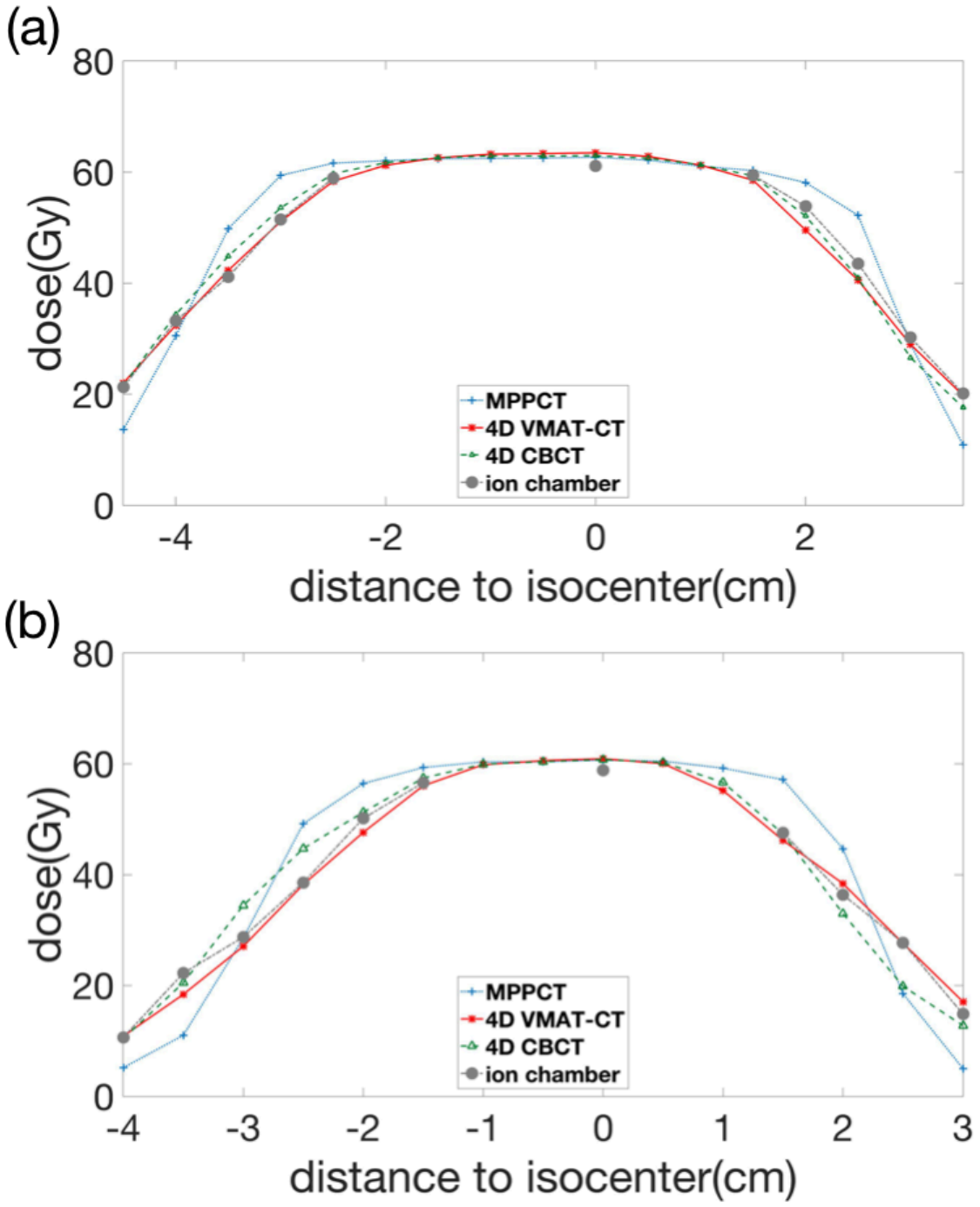


Figure 3.7. Point dose comparison of ion chamber measurements with calculated doses at the same positions based on MPPCT, 4D VMAT-CT+ and 4D CBCT for (a) 4D Union plan with regular breathing pattern, (b) initial 4D ART plan with regular breathing pattern, (c) 4D Union plan with irregular breathing pattern, and (d) initial 4D ART initial plan with irregular breathing pattern.
(figure cont'd)

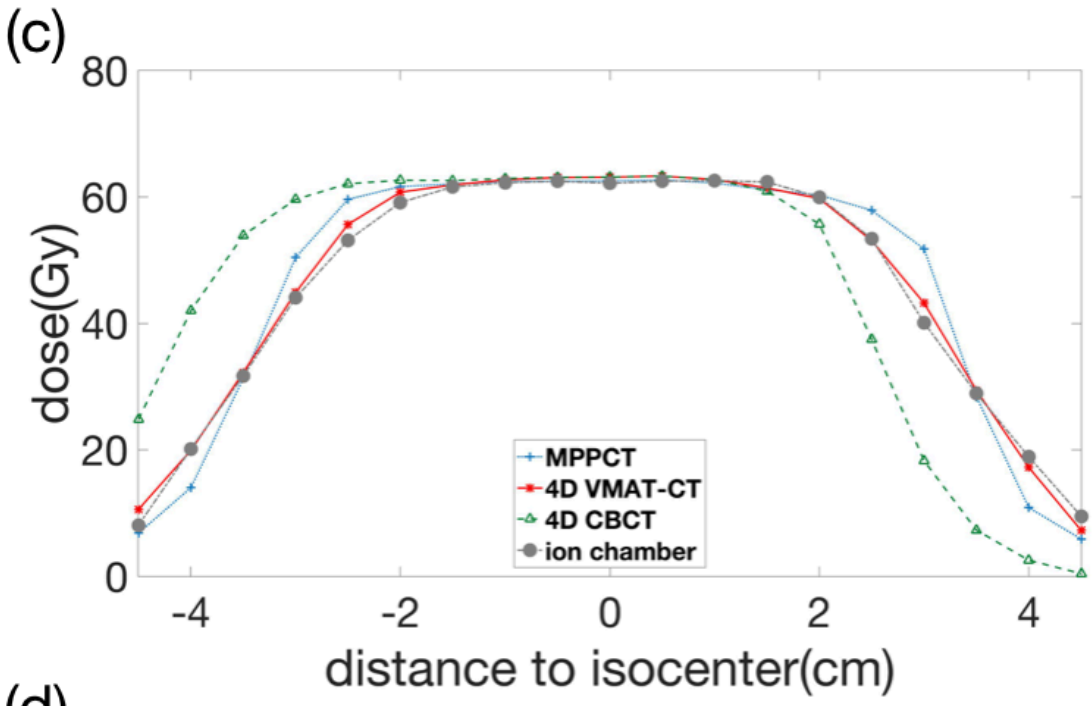
(c)
80
60
40
20
0
dose(Gy)
MPPCT
4D VMAT-CT
4D CBCT
ion chamber
-4
-2
0
2
4
distance to isocenter(cm)

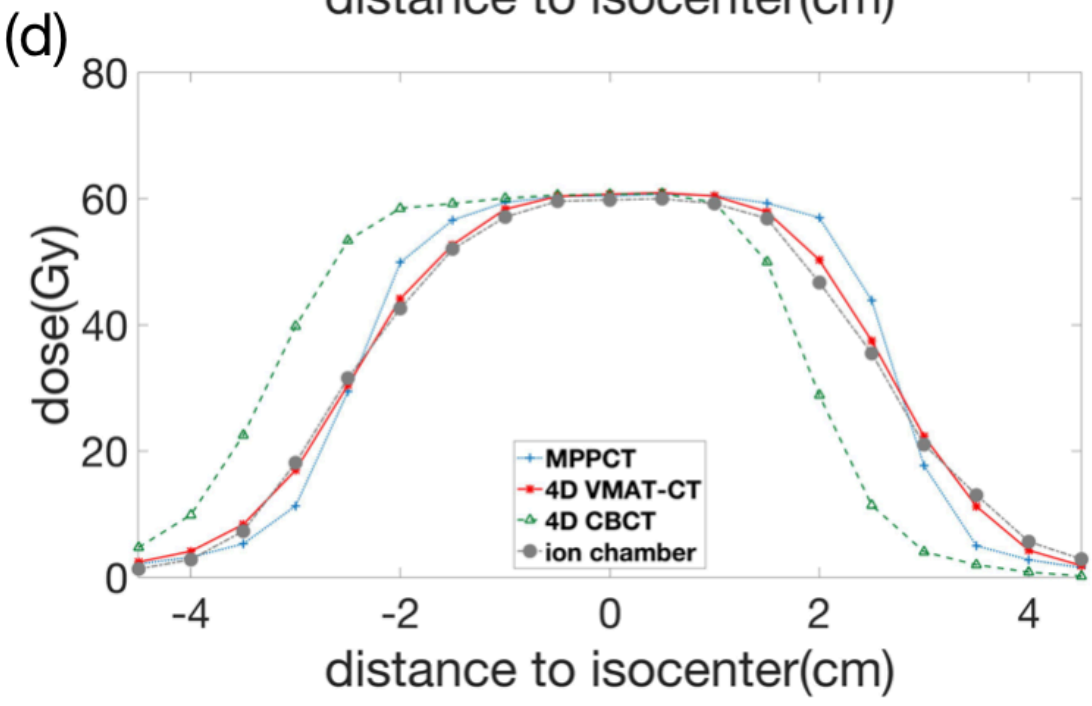
(d)
80
60
40
20
0
dose(Gy)
MPPCT
4D VMAT-CT
4D CBCT
ion chamber
-4
-2
0
2
4
distance to isocenter(cm)

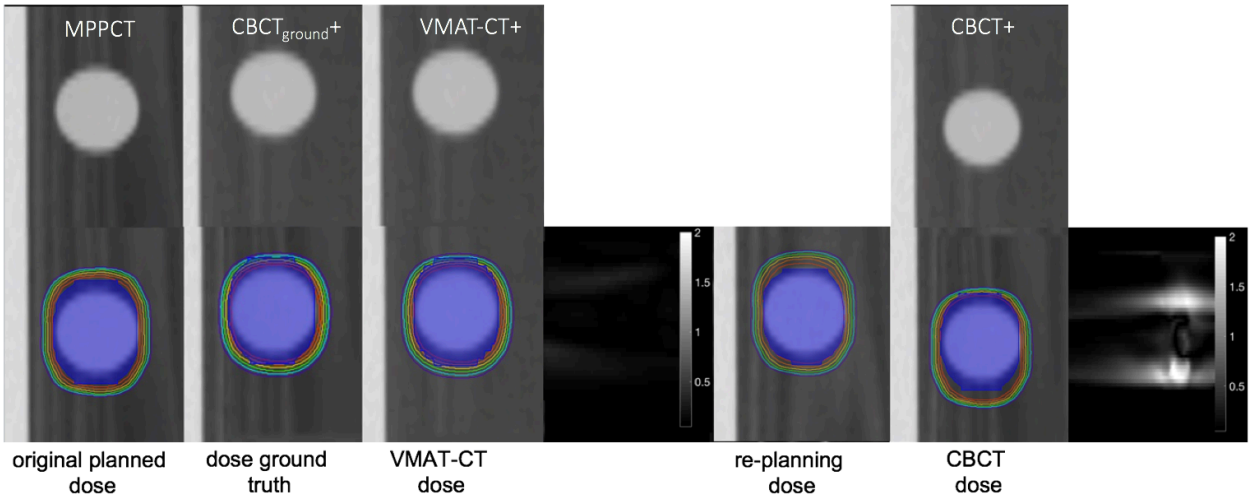


Figure 3.8. ART demonstrated on the Quasar phantom. (Top row) comparison of MPPCT, CBCT$_{ground}$+ (registered MPPCT/CBCT$_{ground}$), VMAT-CT+, CBCT+ (registered MPPCT/pre-treatment CBCT); (bottom row) dose distributions in the original plan, dose after change of breathing pattern based on CBCT$_{ground}$, dose after change of breathing pattern based on VMAT-CT+, 3D Gamma plot of comparison between VMAT-CT dose and dose ground truth, re-optimized dose based on VMAT-CT+, dose based on pre-treatment CBCT with a different breathing pattern compared to the ground truth mimicking a possible breathing pattern change before and during beam-on, and 3D Gamma plot of comparison between CBCT dose and dose ground truth. The blue shaded area is the original or new PTV contour.

Figure 3.9. shows dose calculation and adaptive replanning for the in-house 4D deformable phantom. VMAT-CT can track the phantom's deformation and change of respiratory pattern correctly compared with ground truth (Gamma passing rate 100%), while pre-treatment CBCT cannot (Gamma passing rate 95.5%). The PTV had 95% coverage of the prescription dose in the original 4D ART plan, dropped to 93% after phantom deformation and change of respiratory pattern, but went up to 95% after re-planning. New margin of the PTV compared to the old margin of PTV showed 1 mm expansion in superior direction and 1 mm shrinkage in inferior direction.

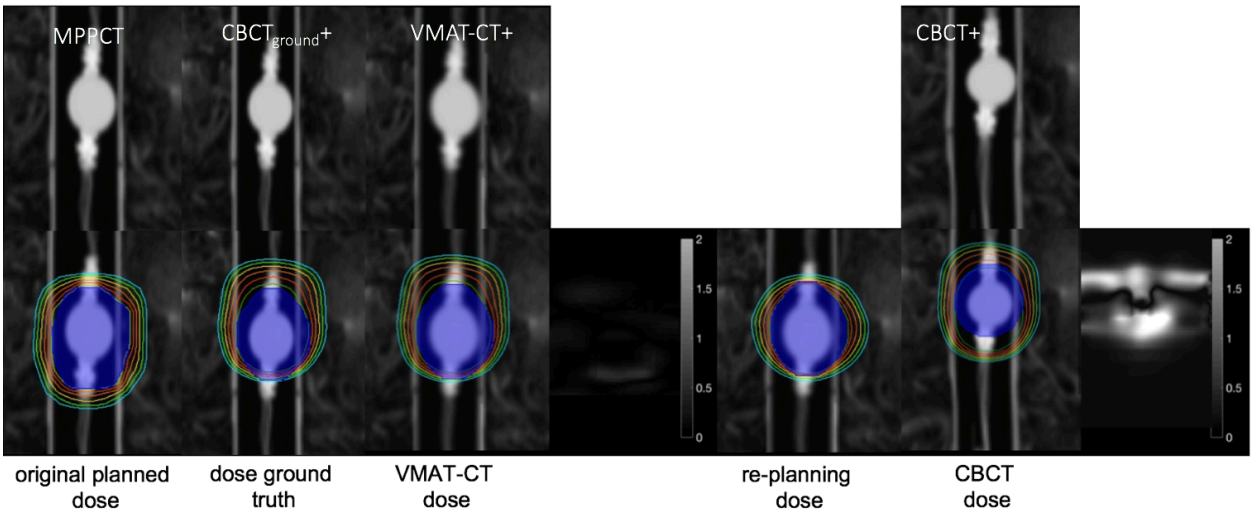


Figure 3.9. ART demonstrated on the in-house 4D deformable phantom. (Top row) comparison of MPPCT, CBCT$_{ground}$+ (registered MPPCT/CBCT$_{ground}$), VMAT-CT+, CBCT+ (registered MPPCT/pre-treatment CBCT); (bottom row) dose distributions in the original plan, dose after deformation based on CBCT$_{ground}$, dose after deformation based on VMAT-CT+, 3D Gamma plot of comparison between VMAT-CT dose and dose ground truth, re-optimized dose based on VMAT-CT+, dose based on pre-treatment CBCT with a different breathing pattern and a different deformation compared to the ground truth mimicking a possible breathing pattern change and a possible deformation change before and during beam-on, and 3D Gamma plot of comparison between CBCT dose and dose ground truth. The blue shaded area is the original or deformed PTV contour.

Figure 3.10. shows the result of geometry change and dose calculations for the SBRT lung patient. In Figure 3.10.(a), 4D VMAT-CT showed good agreement with 4D CT where from peak to peak's center of mass both shifted about 8mm. In Figure 3.10. (b), the PTV in the original plan is maximum intensity projection (Thorwarth *et al.*) plus 5mm margin, and the PTV has a 95.8% coverage of the prescription dose in the original plan; while for 4D VMAT-CT based PTV showed the mean position PTV, and it has a 2mm shrinkage in the superior direction and a 5mm shrinkage in the inferior direction, and the PTV has a 98.5% coverage of the prescription dose, which indicates no need to re-plan. The 3D gamma passing rate between 4D VMAT-CT based dose to the original planned dose is 99.7%. VMAT-CT+ showed target position was closer to diaphragm since there was a slight baseline change and phase 2 and phase 4 were closer to phase 3 compared

to the 4D CT. Therefore, diaphragm received more dose compared to planned dose in VMAT-CT based dose calculation.

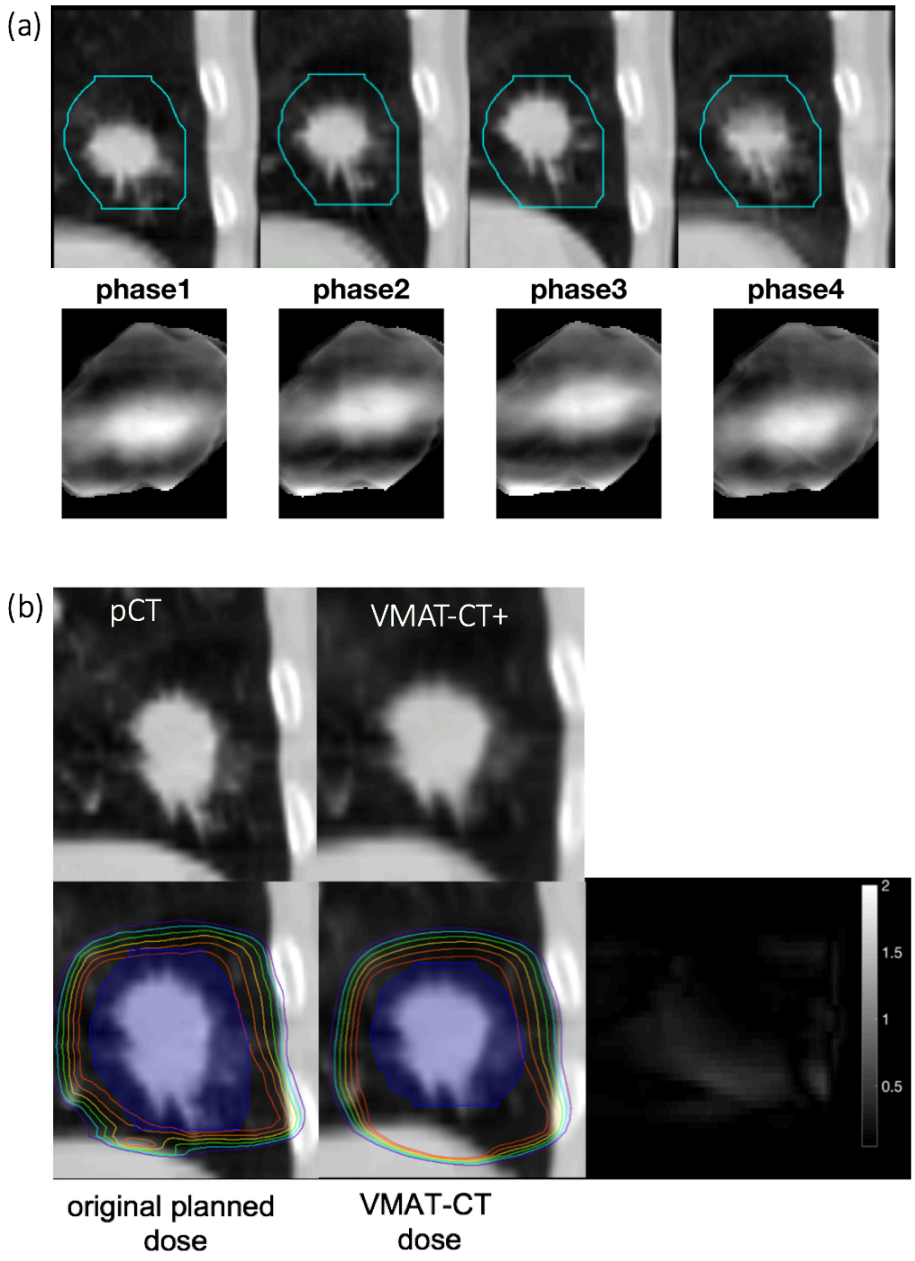


Figure 3.10. Dose comparison on SBRT patient. (a) comparison between 4D CT and 4D VMAT-CT. (b) (Top row) comparison of planning CT, mean position VMAT-CT+; (bottom row) dose distributions in the original plan, dose based on 4D VMAT-CT+, 3D Gamma plot of comparison between 4D VMAT-CT dose and original planned dose, and 3D Gamma plot of comparison between 4D VMAT-CT dose and original planned dose. The blue shaded area is the original or deformed PTV contour.

Table 3.1. shows rigid registration uncertainties from registering each phase's VMAT-CT to MPPCT, and each try is the averaged result from 4 phases. Table 3.2 shows the deformable registration uncertainties. The largest potential point dose uncertainty from rigid registration by shifting the MPPCT the mean uncertainty in each direction is 2.59, 0.60 and 2.65Gy for x, y and z-direction respectively by using the 4D ART plan. The 3D gamma passing rate after shifting the MPPCT the mean uncertainty in each direction are all 100%. For the deformable registration, the expansion of the mean HD reduces the mean PTV dose by 4.41Gy while the shrinkage increases the mean PTV by 4.41Gy by using the 4D ART plan for both situations. The 3D gamma passing rate after expansion or shrinkage are both 99.8%.

Table 3.1. Rigid registration error when planning CT is registered to VMAT-CT. SD: standard deviation.

| Tries | X (mm) | Y (mm) | Z (mm) | Total (mm) |
|---|---|---|---|---|
| 1 | 0.183 | 0.133 | 0.444 | 0.498 |
| 2 | 0.138 | 0.171 | 0.330 | 0.396 |
| 3 | 1.953 | 0.395 | 0.614 | 2.085 |
| 4 | 2.054 | 0.286 | 0.916 | 2.267 |
| Mean | 1.082 | 0.246 | 0.576 | 1.312 |
| SD | 1.065 | 0.119 | 1.255 | 1.002 |

Table 3.2. Deformable registration error when planning CT is registered to VMAT-CT. SD: standard deviation.

| Phases | HD (mm) | MDA (mm) | DSC | Jaccard coefficient |
|---|---|---|---|---|
| 1 | 1.840 | 0.455 | 0.928 | 0.866 |
| 2 | 1.481 | 0.340 | 0.950 | 0.905 |
| 3 | 1.774 | 0.438 | 0.938 | 0.883 |
| 4 | 1.215 | 0.227 | 0.967 | 0.935 |
| Mean | 1.578 | 0.365 | 0.946 | 0.897 |
| SD | 0.288 | 0.105 | 0.017 | 0.030 |

## 3.4. Discussion

We demonstrated the feasibility of geometry and dose tracking of 4D lung SBRT based on 4D VMAT-CT and the potential for ART. Compared to the previous study (Kida *et al.*, 2011), we did not set contains on MLC movement, which is the case for all clinical patients, and we were still able to trace respiratory signal and sort EPID images and Linac log into 4 phases. We also registered VMAT-CT with MPPCT to create VMAT-CT+ so that we can have the full FOV and have the electron density information for dose calculation. One small drawback of this study compared to Kida *et al.* (Kida *et al.*, 2011) is that we did not have in-treatment 4D CBCT as the ground truth as in-treatment CBCT is not available in most clinics, but we used ion chamber measurements and 4D $CBCT_{ground}$ instead and obviously these methods are not feasible for real patients.

Previous studies reported amplitude-based sorting shows superior results than time-based sorting (Lu *et al.*, 2006; Wink *et al.*, 2006; Kavanagh *et al.*, 2009). However, there are usually 200 images for a full arc SBRT beam, and each phase only has 50 images using time-based sorting. If amplitude-based sorting is used, there could be a big difference in the number of images in each phase because there are more images in end-inhale or end-exhale phase when tumor slows down and there are fewer images in the middle phases when tumor moves faster. Middle-phase VMAT-CT will then have poorer image quality compared to the end-exhale/inhale phase. In addition, NCC method may not always detect amplitude correctly because sometimes blurry images or blockage from the MLC would generate a wrong amplitude of target movement, so amplitude- based sorting could introduce even more uncertainties. If the sampling rate of EPID image could be increased in the future, we can have less blurry image and more high-quality images, and amplitude-based sorting could be a possibility then.

We determined NCC and time-based sorting are not sources of uncertainties. We compared NCC detected respiratory signal side by side with EPID images to make sure the detected shift direction is the same as the direction of target movement since the movement of the target on EPID images is quite visible. When EPID image is blurry, NCC sometimes cannot generate an accurate shift in two consecutive images, so we can manually override the result by either estimating a visible marker's shift or just setting it to zero. When MLC blocks out the target, NCC cannot detect the right signal and we will manually override the result to zero. As mentioned before in the method, the missing signal would be made up with Fourier transformation since these frequencies does not fall within the band pass filter threshold. Either case it will not interfere with the final reconstruction result since it is only very few slices compared to the total image number. If certain image (at most a few) is sorted into the wrong phase using time-based sorting, which will be more likely in middle phases because target moves faster in those phases and sorting is slightly more error-prone, it will not make a big difference because the number of wrong images is a very small fraction of the total number of images, and the images in middle phases are usually already a little blurrier since the target moves faster and the range of target motion is wider in middle phase than in peak phase. We also verified the NCC method and time-based sorting using 8 patient beams and the results are all accurate compared to the ground truth.

We did verify the difference between dose based on $CBCT_{ground}$ and dose based on VMAT-CT or the ion chamber measurement is minimum when we fed the same irregular breathing pattern before and after beam-on time, and this is why we can use $CBCT_{ground}$ as the dose reference in Figure 3.8. and Figure 3.9.. Theoretically, there would be some different because even though the signals fed to the Quasar phantom before and after beam-on have the same amplitude and period, the starting phase of the signals would be different and there is a synchronization issue. The error

brought by synchronization is minimum here, which is possibly because the breathing patterns we chose are roughly symmetric along the baseline instead of being heavily swayed to one side. When we used 4D $CBCT_{ground}$ to validate 4D dose reconstruction for the deformable phantom, the MLC control points were almost evenly distributed in four phases because of the uniform distribution of breathing signal. However, if two very different breathing patterns, i.e. one of them is heavily swayed to one side but the other is not, were fed to the Quasar phantom before and after beam delivery, the effect of dose error brought by using respiratory signal extracted from CBCT would be more apparent since the signal does not represent the true motion during beam delivery.

The reason CBCT-based dose does not differ that much from VMAT-CT based dose and the ground truth for regular breathing pattern (Figure 3.7.(a), (b)) is that MU delivery is quite even with time and MLC aperture shape does not change that much with time either for SBRT plan. For regular sine breathing pattern, the target spent about the same amount of time in each phase and difference in the initial phase shift will not change composite dose significantly. However, for irregular breathing pattern, because CBCT cannot detect the possible change of breathing pattern before and after beam delivery, dose discrepancy due to inaccurate respiratory signal is magnified and CBCT-based dose has a large discrepancy from VMAT-CT based dose or the ground truth (Figure 3.7.(c),(d)).

When the target moved away from the mean position, for the 4D Union plan, the 5 mm area we added after MIP would travel outside of the edge of the beam when the target moves close to the peak; for offline adaptive plan, part of the target that was close to the edge of the beam and was originally in the beam would be outside the beam for a portion of the treatment when it travels close to the peak. As the target constantly traveled outside the beam due to breathing, the edge of the PTV would not receive the expected dose and would have a dose fall-off. For the irregular

breathing pattern, the target did not travel to the full extent of the maximum amplitude and was still within beam's edge in many cycles, while the regular breathing pattern had more fraction of time spent close to the maximum amplitude. This is why the fall-off shoulder in the irregular breathing pattern (4 mm) is smaller than that in the regular breathing pattern (5 mm) (Figure 3.7.). This dose fall-off appeared not only in 4D ART plans, but also in 4D union plans. In our 4D union plan, GTV is 3 cm, the amplitude of the movement on each side is 1cm, MIP only covers the path of GTVso is 5 cm, PTV is MIP plus 5mm on each side and is 6 cm. The dose fall-off happened at the 5-mm margin added to the MIP, which means the outer 1cm of PTV received less than the prescription dose 50Gy. However, the 5-cm MIP did receive 50Gy, which means the GTV still received the prescription dose and it was the area correlated to the margin traveled outside the beam edge did not receive the full prescription dose. To improve upon 4D union which is overshooting healthy tissues and the ART plan proposed by Harsolifa *et al.* (Harsolia *et al.*, 2008) which barely covers the GTV (for irregular breathing pattern, by comparing the VMAT-CT based dose to prescription dose 50Gy in Figure 3.7.(d), there is 3.15cm of margin over 50Gy, which is barely bigger than the 3cm GTV; 3.15cm is acquired from the difference between the two intersections between 4D VMAT-CT dose to y=50Gy.) and may underdose the subclinical disease, we recommend calculating the ART margin from the convolution of CTV with PDF, and adding a 5-mm additional margin to the ART margin for the possible dose fall-off caused by the movement. When this kind of plan is delivered, only the desired region will get prescription dose and healthy tissue will not be overshoot.

Previously ART was usually done using CBCT on the same day (6). CBCT is taken before treatment, so it cannot detect geometry change or deformation happen after CBCT is taken, and it is common the breathing pattern will have some degree of change before and after beam is on.

Besides, 4D CBCT significantly increases patient dose (8). One of the major advantage of our study is that VMAT-CT can give the information on in-treatment respiratory signal and does not require any external markers. Compared to Harsolia *et al.* (Harsolia *et al.*, 2008) which used daily fluoroscopy for ART plans and obviously fluoroscopy will introduce significant extra imaging dose, our method introduces no extra imaging dose since VMAT-CT came directly from treatment beams.

In the future, we will evaluate our method in more patient studies and the possibility of improving image quality on different machines with a higher quality image panel or a faster EPID sampling rate. If the EPID panel can capture images with better image quality, the image quality of reconstructed VMAT-CT can certainly be improved. If the EPID panel has a faster sampling rate, it is possible to sort images to more than four phases and use amplitude-based image sorting to improve image sorting and reduce blurry in each phase.

## 3.5. Conclusion

4D VMAT-CT was reconstructed under more stringent and clinically realistic conditions, 4D dose was calculated with in-treatment geometry in each phase and deformably registered to get the composite dose, and ART was carried out when prescription dose was not met. Overall 4D VMAT-CT can be a very promising tool for respiratory signal tracking, patient positioning, tumor targeting, normal tissue sparing and treatment QA without introducing any extra dose.

# 4. CONCLUSIONS

This work reports accurate tracking of position and dose during VMAT based on VMAT-CT.

Previous studies showed the application of VMAT-CT is limited because it has limited field of view and no density information. In addition, the new generation of multi-leaf collimator with faster speed and various collimator angles used in patients' plans could cause more artifacts in VMAT-CT. Therefore, in chap 2, we extended VMAT-CT concept, generated complete three-dimensional (3D) CT images by registering planning CT to VMAT-CT, calculated new 3D dose. Tracking based on planning CT, VMAT-CT+, and CBCT were compared. When prescription dose was not met for planning target volume (PTV), re-planning was demonstrated on an in-house deformable phantom. Criteria for VMAT-CT reconstruction and possible uncertainties were also evaluated. Application of the workflow was also demonstrated on a 3D lung VMAT patient. Overall, we demonstrated the feasibility of three-dimensional (3D) tracking and ART based on VMAT-CT.

However, 3D VMAT-CT is not suitable for treatments like lung stereotactic body radiotherapy (SBRT) that involve significant target movement due to patient breathing. Therefore, in chap 3, we demonstrated feasibility of 4D tracking and ART based on 4D VMAT-CT. A QUASAR respiratory phantom and an in-house deformable lung phantom were used in this study and clinically realistic SBRT lung plans, including 4D union plan and 4D ART plan, were generated for the phantoms. Breathing signal was extracted from electronic portal imaging device (EPID) images acquired during VMAT delivery using normalized cross correlation method. Synchronized EPID images and Linac log were both sorted out into four phases, and VMAT-CT+ was generated in each phase by fusing reconstructed VMAT-CT and planning CT using rigid or

deformable registration. Dose was calculated in each phase and was registered to the mean position planning CT for 4D dose reconstruction, and the composite dose was validated. ART was demonstrated on the phantoms when planning goal was not met. Potential uncertainties were also evaluated. Application of the workflow was also demonstrated on a 4D lung SBRT patient.

## 4.1. Implications

The works presented in this dissertation suggest that it is feasible to accurately track position and dose during VMAT treatment based on VMAT-CT. Phantom study also suggest that it is feasible to adapt the plan based on VMAT-CT. Patient study suggests that dose discrepancy compared to the original dose does not happen very often.

The result of this work may find clinical applications in daily routine for patients that fit the reconstruction criteria. It can retrospectively verify the geometry and dose delivered during treatment.

For 3D VMAT patient, as long as the site has good contrast, meaning there is some air or bone in the PTV, then it is possible to verify if the PTV region has any geometry change after patient setup and during treatment and also to verify if the PTV received enough prescription dose. However, the field of view of VMAT-CT is only limited to the PTV region and it cannot track any other parts of the patients' geometry change and cannot verify any organ at risk's dose. The 3D workflow can benefit patients of different cancer sites, including head and neck, esophagus, lung, pancreatic, and prostate. However, for pancreatic and prostate patients, in order for VMAT-CT to show any kind of information, the site needs to have some markers distinct from soft tissue, like tube after surgery, or prostate seeds and femoral heads.

For 4D SBRT patients, it is especially useful to extract the respiratory signal directly from EPID images during treatment without any external surrogate or any extra dose. From the breathing pattern during treatment, we can verify if the margin from the original plan is sufficient so that even with free breathing, the target still receives enough prescription dose. For lung patients, they already have good contrast in the PTV region. This workflow can easily be incorporated into daily clinical routine for SBRT lung patients since there is no monitoring of their in-treatment breathing pattern in a lot of clinics. Another advantage of this methodology is that the only equipment needed is EPID panel, which modern linacs already have.

## 4.2. Coherence with literature

The VMAT-CT reconstruction demonstrated showed generally good agreement with previous literature. However, the workflow demonstrated cannot be directly compared with literature since previous literature did not expand the VMAT-CT concept to larger field of view and dose calculation.

Previously, VMAT-CT reconstruction was demonstrated on MLCi2 head with non-clinically realistic collimator angles (Poludniowski *et al.*, 2010). We can replicate the result with the same machine. However, newer Linac heads with faster MLC movement and faster gantry rotation speed requires the reconstruction algorithm to accommodate these stringent conditions. Besides, almost all clinical plans use non-zero-degree collimator angle, which makes it necessary to introduce the collimator rotation matrix in chap 2.

Another previous work on 4D VMAT-CT was demonstrated with very slow MLC speed, which makes the plan clinically unrealistic as well (Kida *et al.*, 2011). We can replicate the result as well. By testing different input signal on the Quasar phantom, respiratory signal extracted from

EPID images has good agreement with input signal, and 4D VMAT-CT reconstruction is feasible with time-based sorting, which are all in accordance with study by Kida *et al.* (2011).

Previously ART was usually done on same day CBCT (Sonke and Belderbos, 2010). However, CBCT cannot detect respiratory change during treatment. Besides, 4D CBCT significantly increases patient dose (Cooper *et al.*, 2019a). Compared to Harsolia *et al.* (Harsolia *et al.*, 2008) which used daily fluoroscopy for ART plans and obviously fluoroscopy will introduce significant extra imaging dose, our method introduces no extra imaging dose since VMAT-CT came directly from treatment beams.

## 4.3. Future work

In the future, we will focus on three possible directions: improve image quality, speed up processing time, and evaluate our method in more patient studies.

First, we want to explore the possibility of improving image quality on different machines with a higher quality image panel or a faster EPID sampling rate and with iterative reconstruction algorithm. If the EPID panel can capture images with better image quality, the image quality of reconstructed VMAT-CT can certainly be improved. If the EPID panel has a faster sampling rate, it is possible to sort images to more than four phases and use amplitude-based image sorting to improve image sorting and reduce blurry in each phase. With iterative reconstruction algorithm, it is possible to improve image quality with limited EPID hardware situation.

Second, we want to speed up the time for the entire workflow. One of the drawbacks of the study is the long processing time. The reconstruction of VMAT-CT is usually done around an hour for one 3D volume. The reconstruction time for 4D VMAT-CT can take a lot longer. The entire workflow for 3D plans usually takes about one day, while the workflow for 4D plans can take at

least two days. This is largely due to the fact that the process of registration and generating VMAT-CT+ and new beam delivery file are all done manually. One possibility to speed up the process is to implement the entire workflow automatically with only manual check on deformable registration.

Last but not least, in the future we want to acquire more patients and ultimately incorporate the workflow into daily clinical routine. With more patient data, it is possible to see what type of patients may subject to the most movement or geometry change during treatment and are more beneficial from the study.

## LIST OF REFERENCES


Bras S and Pinho A J 2015 ECG biometric identification: A compression based approach *Conference proceedings : ... Annual International Conference of the IEEE Engineering in Medicine and Biology Society. IEEE Engineering in Medicine and Biology Society. Annual Conference* **2015** 5838-41

Brenner D, Elliston C, Hall E and Berdon W 2001 Estimated risks of radiation-induced fatal cancer from pediatric CT *AJR Am J Roentgenol* **176** 289-96

Brenner D J, Doll R, Goodhead D T, Hall E J, Land C E, Little J B, Lubin J H, Preston D L, Preston R J, Puskin J S, Ron E, Sachs R K, Samet J M, Setlow R B and Zaider M 2003 Cancer risks attributable to low doses of ionizing radiation: assessing what we really know *Proceedings of the National Academy of Sciences of the United States of America* **100** 13761-6

Brenner D J and Elliston C D 2004 Estimated radiation risks potentially associated with full-body CT screening *Radiology* **232** 735-8

Brenner D J and Hall E J 2007 Computed tomography--an increasing source of radiation exposure *N Engl J Med* **357** 2277-84

Bressane A, Roveda J A and Martins A C 2015 Statistical analysis of texture in trunk images for biometric identification of tree species *Environmental monitoring and assessment* **187** 212

Brock K K, Mutic S, McNutt T R, Li H and Kessler M L 2017 Use of image registration and fusion algorithms and techniques in radiotherapy: Report of the AAPM Radiation Therapy Committee Task Group No. 132 *Med Phys* **44** e43-e76

Cebi A, Akgun E, Ozturk T and Avci E 2018 Cancer Statistics in Giresun Province, Turkey: A 12-Years Retrospective Review *The Gulf journal of oncology* **1** 43-8

Chodick G, Ronckers C M, Shalev V and Ron E 2007 Excess lifetime cancer mortality risk attributable to radiation exposure from computed tomography examinations in children *The Israel Medical Association journal : IMAJ* **9** 584-7

Cooper B J, O'Brien R T, Shieh C-C and Keall P J 2019a Real-time respiratory triggered four dimensional cone-beam CT halves imaging dose compared to conventional 4D CBCT *Physics In Medicine And Biology* **64** 07NT1-NT1

Cooper B J, O'Brien R T, Shieh C C and Keall P J 2019b Real-time respiratory triggered four dimensional cone-beam CT halves imaging dose compared to conventional 4D CBCT *Phys Med Biol* **64** 07NT1

Defoor D L, Vazquez-Quino L A, Mavroidis P, Papanikolaou N and Stathakis S 2015 Anatomy-based, patient-specific VMAT QA using EPID or MLC log files *J Appl Clin Med Phys* **16** 5283

DelPozo-Banos M, Travieso C M, Weidemann C T and Alonso J B 2015 EEG biometric identification: a thorough exploration of the time-frequency domain *Journal of neural engineering* **12** 056019

Essers M and Mijnheer B J 1999 In vivo dosimetry during external photon beam radiotherapy *Int J Radiat Oncol Biol Phys* **43** 245-59

Faridani A, Buglione K A, Huabsomboon P, Iancu O D and McGrath J 2001 Introduction to local tomography *Contemporary Mathematics* **278** 29-48

Goodman T R and Amurao M 2012 Medical imaging radiation safety for the female patient: rationale and implementation *Radiographics : a review publication of the Radiological Society of North America, Inc* **32** 1829-37

Gradishar W J, Stephenson P, Glover D J, Neuberg D S, Moore M R, Windschitl H E, Piel I and Abeloff M D 2001 A Phase II trial of cisplatin plus WR-2721 (amifostine) for metastatic breast carcinoma: an Eastern Cooperative Oncology Group Study (E8188) *Cancer* **92** 2517-22

Green O L, Henke L E and Hugo G D 2019 Practical Clinical Workflows for Online and Offline Adaptive Radiation Therapy *Seminars in Radiation Oncology* **29** 219-27

Haghighat M, Zonouz S and Abdel-Mottaleb M 2015 CloudID: Trustworthy cloud-based and cross-enterprise biometric identification *Expert Systems with Applications* **42** 7905-16

Harsolia A, Hugo G D, Kestin L L, Grills I S and Yan D 2008 Dosimetric advantages of four-dimensional adaptive image-guided radiotherapy for lung tumors using online cone-beam computed tomography. pp 582-9

Heinzerling J H, Anderson J F, Papiez L, Boike T, Chien S, Zhang G, Abdulrahman R and Timmerman R 2008 Four-dimensional computed tomography scan analysis of tumor and organ motion at varying levels of abdominal compression during stereotactic treatment of lung and liver *International Journal Of Radiation Oncology, Biology, Physics* **70** 1571-8

Herbert C, Kwa W, Nakano S, James K, Moiseenko V, Wu J, Schellenberg D and Liu M 2013 Stereotactic body radiotherapy: volumetric modulated arc therapy versus 3D non-coplanar conformal radiotherapy for the treatment of early stage lung cancer *Technol Cancer Res Treat* **12** 511-6

Jafarinejad-Farsangi S, Farazmand A, Mahmoudi M, Gharibdoost F, Karimizadeh E, Noorbakhsh F, Faridani H and Jamshidi A R 2015 MicroRNA-29a induces apoptosis via increasing the Bax: Bcl-2 ratio in dermal fibroblasts of patients with systemic sclerosis *Autoimmunity* **48** 369-78

Jin Y J, Dogra R, Cheong I W and Kwak G 2015 Fluorescent Molecular Rotor-in-Paraffin Waxes for Thermometry and Biometric Identification *ACS applied materials & interfaces* **7** 14485-92

Kavanagh A, Evans P M, Hansen V N and Webb S 2009 Obtaining breathing patterns from any sequential thoracic x-ray image set *Phys Med Biol* **54** 4879-88

Kida S, Masutani Y, Yamashita H, Imae T, Matsuura T, Saotome N, Ohtomo K, Nakagawa K and Haga A 2012 In-treatment 4D cone-beam CT with image-based respiratory phase recognition *Radiological physics and technology* **5** 138-47

Kida S, Saotome N, Masutani Y, Yamashita H, Ohtomo K, Nakagawa K, Sakumi A and Haga A 2011 4D-CBCT reconstruction using MV portal imaging during volumetric modulated arc therapy *Radiother Oncol* **100** 380-5

Kuse M, Wang Y F, Kalasannavar V, Khan M and Rajpoot N 2011 Local isotropic phase symmetry measure for detection of beta cells and lymphocytes *Journal of pathology informatics* **2** S2

Kyoso M 2015 Biometric identification with high frequency electrocardiogram: Unregistered user refusal method and performance evaluation *Conference proceedings : ... Annual International Conference of the IEEE Engineering in Medicine and Biology Society. IEEE Engineering in Medicine and Biology Society. Annual Conference* **2015** 2816-9

Lee L, Le Q T and Xing L 2008 Retrospective IMRT dose reconstruction based on cone-beam CT and MLC log-file *Int J Radiat Oncol Biol Phys* **70** 634-44

Li X A 2011 *Adaptive Radiation Therapy* (Boca Raton, FL: CRC Press)

Liang B, Liu B, Zhou F, Yin F F and Wu Q 2016 Comparisons of volumetric modulated arc therapy (VMAT) quality assurance (QA) systems: sensitivity analysis to machine errors *Radiat Oncol* **11** 146

Lin E C 2010 Radiation risk from medical imaging *Mayo Clinic proceedings* **85** 1142-6; quiz 6

Ling C C, Zhang P, Archambault Y, Bocanek J, Tang G and Losasso T 2008 Commissioning and quality assurance of RapidArc radiotherapy delivery system *Int J Radiat Oncol Biol Phys* **72** 575-81

Low D A, Harms W B, Mutic S and Purdy J A 1998a A technique for the quantitative evaluation of dose distributions *Medical Physics* **25** 656-61

Low D A, Harms W B, Mutic S and Purdy J A 1998b A technique for the quantitative evaluation of dose distributions *Med Phys* **25** 656-61

Lu V M, Welby J P, Laack N N, Mahajan A and Daniels D J 2020 Pseudoprogression after radiation therapies for low grade glioma in children and adults: A systematic review and meta-analysis *Radiotherapy and Oncology* **142** 36-42

Lu W, Parikh P J, Hubenschmidt J P, Bradley J D and Low D A 2006 A comparison between amplitude sorting and phase-angle sorting using external respiratory measurement for 4D CT *Med Phys* **33** 2964-74

Mans A, Remeijer P, Olaciregui-Ruiz I, Wendling M, Sonke J J, Mijnheer B, van Herk M and Stroom J C 2010 3D Dosimetric verification of volumetric-modulated arc therapy by portal dosimetry *Radiother Oncol* **94** 181-7

McGrath S D, Matuszak M M, Yan D, Kestin L L, Martinez A A and Grills I S 2010 Volumetric modulated arc therapy for delivery of hypofractionated stereotactic lung radiotherapy: A dosimetric and treatment efficiency analysis *Radiother Oncol* **95** 153-7

Mijnheer B, Beddar S, Izewska J and Reft C 2013 In vivo dosimetry in external beam radiotherapy *Med Phys* **40** 070903

Murphy M J, Balter J, Balter S, BenComo J A, Jr., Das I J, Jiang S B, Ma C M, Olivera G H, Rodebaugh R F, Ruchala K J, Shirato H and Yin F F 2007 The management of imaging dose during image-guided radiotherapy: report of the AAPM Task Group 75 *Med Phys* **34** 4041-63

Ong C L, Verbakel W F, Cuijpers J P, Slotman B J, Lagerwaard F J and Senan S 2010 Stereotactic radiotherapy for peripheral lung tumors: a comparison of volumetric modulated arc therapy with 3 other delivery techniques *Radiother Oncol* **97** 437-42

Otto K 2008 Volumetric modulated arc therapy: IMRT in a single gantry arc *Med Phys* **35** 310-7

Palma D A, Verbakel W F, Otto K and Senan S 2010 New developments in arc radiation therapy: a review *Cancer Treat Rev* **36** 393-9

Poludniowski G, Thomas M D, Evans P M and Webb S 2010 CT reconstruction from portal images acquired during volumetric-modulated arc therapy *Phys Med Biol* **55** 5635-51

Popple R A, Balter P A and Orton C G 2014 Point/Counterpoint. Because of the advantages of rotational techniques, conventional IMRT will soon become obsolete *Med Phys* **41** 100601

Poulsen P R, Schmidt M L, Keall P, Worm E S, Fledelius W and Hoffmann L 2012 A method of dose reconstruction for moving targets compatible with dynamic treatments. pp 6237-46

Premo C, Apolo A B, Agarwal P K and Citrin D E 2015 Trimodality Therapy in Bladder Cancer: Who, What, and When? *Urologic Clinics of North America* **42** 169-80

Prevost J B, Voet P, Hoogeman M, Praag J, Levendag P and Nuyttens J J 2008 Four-dimensional stereotactic radiotherapy for early stage non-small cell lung cancer: a comparative planning study *Technol Cancer Res Treat* **7** 27-33

Qian J, Lee L, Liu W, Chu K, Mok E, Luxton G, Le Q T and Xing L 2010 Dose reconstruction for volumetric modulated arc therapy (VMAT) using cone-beam CT and dynamic log files *Phys Med Biol* **55** 3597-610

Ricardi U, Badellino S and Filippi A R 2015 Stereotactic radiotherapy for early stage non-small cell lung cancer *Radiation oncology journal* **33** 57-65

Ron E 2003 Cancer risks from medical radiation *Health Phys* **85** 47-59

Ronckers C M, Land C E, Miller J S, Stovall M, Lonstein J E and Doody M M 2010 Cancer mortality among women frequently exposed to radiographic examinations for spinal disorders *Radiat Res* **174** 83-90

Sapkaroski D, Osborne C and Knight K A 2015 A review of stereotactic body radiotherapy - is volumetric modulated arc therapy the answer? *Journal of medical radiation sciences* **62** 142-51

Sonke J-J and Belderbos J 2010 Adaptive radiotherapy for lung cancer *Seminars In Radiation Oncology* **20** 94-106

Sterpetti A V, Costi U and D'Ermo G 2019 National statistics about resection of the primary tumor in asymptomatic patients with Stage IV colorectal cancer and unresectable metastases. Need for improvement in data collection. A systematic review with meta-analysis *Surgical oncology* **33** 11-8

Storisteanu D M, Norman T L and Grigore A 2015 Biometric fingerprint system to enable rapid and accurate identification of beneficiaries *Global health, science and practice* **3** 135-7

Teoh M, Beveridge S, Wood K, Whitaker S, Adams E, Rickard D, Jordan T, Nisbet A and Clark C H 2013 Volumetric-modulated arc therapy (RapidArc) vs. conventional fixed-field intensity-modulated radiotherapy for (1)(8)F-FDG-PET-guided dose escalation in oropharyngeal cancer: a planning study *Medical dosimetry : official journal of the American Association of Medical Dosimetrists* **38** 18-24

Teoh M, Clark C H, Wood K, Whitaker S and Nisbet A 2011 Volumetric modulated arc therapy: a review of current literature and clinical use in practice *Br J Radiol* **84** 967-96

Thorwarth D, Notohamiprodjo M, Zips D and Muller A C 2017 Personalized precision radiotherapy by integration of multi-parametric functional and biological imaging in prostate cancer: A feasibility study *Z Med Phys* **27** 21-30

Tyagi N, Yang K, Gersten D and Yan D 2012 A real time dose monitoring and dose reconstruction tool for patient specific VMAT QA and delivery *Med Phys* **39** 7194-204

Tyldesley S, Boyd C, Schulze K, Walker H and Mackillop W J 2001 Estimating the need for radiotherapy for lung cancer: an evidence-based, epidemiologic approach *Int J Radiat Oncol Biol Phys* **49** 973-85

Velec M, Moseley J L, Eccles C L, Craig T, Sharpe M B, Dawson L A and Brock K K 2011 Effect of Breathing Motion on Radiotherapy Dose Accumulation in the Abdomen Using Deformable Registration *International Journal of Radiation Oncology, Biology, Physics* **80** 265-72

Verbakel W F, Cuijpers J P, Hoffmans D, Bieker M, Slotman B J and Senan S 2009 Volumetric intensity-modulated arc therapy vs. conventional IMRT in head-and-neck cancer: a comparative planning and dosimetric study *Int J Radiat Oncol Biol Phys* **74** 252-9

Verellen D, De Ridder M, Linthout N, Tournel K, Soete G and Storme G 2007 Innovations in image-guided radiotherapy *Nat Rev Cancer* **7** 949-60

Wendling M, Zijp L J, McDermott L N, Smit E J, Sonke J J, Mijnheer B J and van Herk M 2007 A fast algorithm for gamma evaluation in 3D *Med Phys* **34** 1647-54

Wink N, Panknin C and Solberg T D 2006 Phase versus amplitude sorting of 4D-CT data *J Appl Clin Med Phys* **7** 77-85

Woerner A J, Choi M, Harkenrider M M, Roeske J C and Surucu M 2017 Evaluation of Deformable Image Registration-Based Contour Propagation From Planning CT to Cone-Beam CT *Technol Cancer Res Treat* 1533034617697242

Zhao X and Zhang R 2020 Feasibility of 3D tracking and adaptation of VMAT based on VMAT-CT **Submitted**

# VITA

Xiaodong Zhao was born in Mudanjiang, Heilongjiang to her loving parents. She majored in physics and was selected in the honor class in undergrad at Nanjing University. In her third year of college, she attended a summer school in Tulane University in New Orleans, Louisiana. She then visited Louisiana State University and Mary Bird Perkins Cancer Center where Dr Matthews and Dr Gibbons gave an inspiring speech. This experience convinced her to pursue a career in medical physics. She then went back to China for her last year of college and did her thesis in Monte Carlo simulations in proton.

As a PhD student at Louisiana State University and Agricultural and Mechanical College, she spent most of her time in the clinic. She worked on three different projects during her PhD. The first project is to measure out-of-field dose with TLD. The second project is MR based treatment planning. The third project is an EPID based methodology to verify geometry and dose during VMAT and SBRT treatments. In her spare time, Xiaodong enjoyed playing piano, traveling around the world and cooking to destress.

After graduate school, Xiaodong plans to attend a residency and become a clinical medical physicist. She wishes to continue to give back to the medical physics community.